Genetic polymorphisms in *COMT* and *BDNF* influence synchronization dynamics of human neuronal oscillations

Jaana Simola [*1,2,3¶], Felix Siebenhühner [1¶], Vladislav Myrov [1,4], Katri Kantojärvi [5,6], Tiina Paunio [5,6], J. Matias Palva [1,4,7], Elvira Brattico [8, 9&] & Satu Palva [*1,7&]

[1] Neuroscience Center, Helsinki Institute of Life Science, University of Helsinki, P.O. Box 21, (Haartmaninkatu 3), FI-00014 Helsinki, Finland

[2] Helsinki Collegium for Advanced Studies (HCAS), University of Helsinki, Finland

[3] BioMag Laboratory, HUS Medical Imaging Centre, FI-00029 HUS, Finland.

[4] Department of Neuroscience and Bioengineering (NBE), Aalto University, 02150 Espoo, Finland

[5] Genomics and Biomarkers Unit, Finnish Institute for Health and Welfare, Helsinki, FI-00271 Helsinki, Finland

[6] Department of Psychiatry and SleepWell Research Program, Faculty of Medicine, University of Helsinki and Helsinki University Central Hospital, Helsinki, FI-00014 Helsinki, Finland

[7] Centre for Cognitive Neuroimaging (CCNi), Institute of Neuroscience and Psychology, University of Glasgow, Glasgow G12 8QB, UK.

[8] Center for Music in the Brain (MIB), Department of Clinical Medicine, Aarhus University & The Royal Academy of Music Aarhus/Aalborg, 8000 Aarhus C, Denmark

[9] Department of Education, Psychology, Communication, University of Bari Aldo Moro, 70121 Bari, Italy

* Corresponding authors:

E-mail: jaana.simola@helsinki.fi (JS); satu.palva@helsinki.fi (SP)

¶These authors contributed equally to this work.

&These authors also contributed equally to this work.

Abstract

Neuronal oscillations, their inter-areal synchronization, and scale-free dynamics constitute fundamental mechanisms for cognition by regulating communication in neuronal networks. These oscillatory dynamics have large inter-individual variability that is partly heritable. However, the genetic underpinnings of oscillatory dynamics have remained poorly understood. We recorded resting-state magnetoencephalography (MEG) from 82 healthy participants and investigated whether oscillation dynamics were influenced by genetic polymorphisms in Catechol-O-methyltransferase (*COMT*) Val^{158}Met and brain-derived neurotrophic factor (*BDNF*) Val^{66}Met. Both *COMT* and *BDNF* polymorphisms influenced local oscillation amplitudes and their long-range temporal correlations (LRTCs), while only *BDNF* polymorphism affected the strength of large-scale synchronization. Our findings demonstrate that *COMT* and *BDNF* genetic polymorphisms contribute to inter-individual variability in local and large-scale synchronization dynamics of neuronal oscillations. Comparison of these results to computational modelling of near-critical synchronization dynamics further suggested that *COMT* and *BDNF* polymorphisms influenced local oscillations by influencing the excitation-inhibition balance according to the brain criticality framework.

Introduction

Fast neuronal oscillations (> 1 Hz) and their inter-areal synchronization play fundamental mechanistic roles in cognitive functions by regulating neuronal processing and communication across distributed brain areas (Fries, 2015; Singer, 1999; Womelsdorf et al., 2014). In humans, dynamics of neuronal oscillations and their long-range coherence and phase synchronization, observed non-invasively in magneto- (MEG) and electroencephalography (EEG) recordings, serve fundamental roles in a variety of sensory, motor, and cognitive functions (Fell & Axmacher, 2011; Jensen et al., 2014; Klimesch et al., 2007; Marzetti et al., 2019; Palva & Palva, 2012; Samaha et al., 2020; Siegel et al., 2012; Thut et al., 2012). During rest, brain activity in sub-second time-scales is dominated by alpha oscillations (Klimesch et al., 2007), but involves frequency-specific inter-areal correlation structures throughout the 1–100 Hz range (Arnulfo et al., 2020; Betti et al., 2018; Brookes et al., 2011; Foster et al., 2016; Hipp & Siegel, 2015; Marzetti et al., 2013; Siebenhühner et al., 2020; Zhigalov et al., 2017). Importantly, also the intrinsic spatial organization of spontaneous resting-state functional connectivity (FC) observed with MEG (Betti et al., 2018; Oswald et al., 2017; Siebenhühner et al., 2020), intra-cranial EEG (Arnulfo et al., 2020) and functional magnetic resonance imaging (fMRI) (Hahn et al., 2020; Vidaurre et al., 2021) is predictive of individual variability in task performance, suggesting that such resting-state FC networks reflect underlying individual brain structural organization (Cabral et al., 2014; Mostame & Sadaghiani, 2020).

In addition to fast neuronal dynamics, neuronal activity is characterized by slow (0.1–1 Hz) and infra-slow (0.01–0.1 Hz) fluctuations that are visible in scalp potentials and amplitude envelopes of fast (> 1 Hz) oscillations (Hiltunen et al., 2014; Hipp & Siegel, 2015; Monto et al., 2008). These fluctuations are scale-free, not possessing any predominant temporal scale, and exhibit power-law autocorrelations in their strength known as long-range-temporal correlations

(LRTCs) (Linkenkaer-Hansen et al., 2001; Monto et al., 2008; Palva et al., 2013; Poil et al., 2012; Thiery et al., 2018; Zhigalov et al., 2015). Similarly to instantaneous oscillations dynamics, inter-individual variability in neuronal LRTCs predicts variability in task-related behavioral LRCTs (Palva et al., 2013; Smit et al., 2013), suggesting that they reflect underlying mechanisms of brain functional organization. Indeed, scale-free LRTCs are hallmarks of systems with critical or near-critical dynamics, suggesting that the brain operates near a critical phase transition between disorder and order, *i.e.*, between inadequate and excessive synchronization, respectively (Cocchi et al., 2017).

A large fraction of variability in these fast and slow neuronal dynamics could be heritable and explained by differences in genetic background. MEG spectral power shows similarities between siblings (Leppäaho et al., 2019; Salmela et al., 2016). Twin studies indicate that frontal midline theta activity is genetically related to symptoms and response time variability in Attention-Deficit/Hyperactivity Disorder (ADHD) (McLoughlin et al., 2014) and that peak frequencies (Van Pelt et al., 2012) as well as LRTCs (Linkenkaer-Hansen et al., 2007) of local cortical oscillations have a genetic basis, so that up to 60% of the variance in neuronal LRTCs (Linkenkaer-Hansen et al., 2007) and up to 85% of the variance in cognitive ability (Posthuma et al., 2001) can be attributed to genetic factors. However, what these genetic factors are and how they contribute to the inter-individual variability of synchronization dynamics, including oscillation amplitudes, large-scale synchronization, and LRTCs, have remained central unresolved questions.

One putative factor underlying variability in synchronization dynamics could be genetic polymorphism in genes regulating neuromodulation. Neuromodulation induces alterations in neuronal excitability and neuronal circuit behavior in the time-scale of seconds to minutes (Batista-Brito et al., 2018; Harris & Thiele, 2011; Pfeffer et al., 2021; van den Brink et al., 2018). Compelling evidence indicate that especially the neuromodulatory drive of the catecholamines

dopamine (DA) and noradrenaline (NE) (Cools, 2019; Pfeffer et al., 2021; Robbins & Arnsten, 2009; van den Brink et al., 2018), as well as serotonine (5-hydroxytryptamine; 5-HT) (Harris & Thiele, 2011; Lucki, 1988; Štrac et al., 2016) could constitute an important source for variability in neuronal dynamics by modulating oscillations either via changes of instantaneous activity state or via dynamic state changes on slower timescales (Ferguson & Cardin, 2020; Harris & Thiele, 2011; Lee & Dan, 2012; van den Brink et al., 2019).

Brain DA and NE levels are regulated by their catabolism via COMT enzyme (Männistö & Kaakkola, 1999; Parkin et al., 2018) whose activity is influenced by a common single-nucleotide polymorphism (SNP) in the *COMT* gene substituting methionine (Met) for valine (Val) at codon 158 at sequence 4680 ($Val^{158}Met$ (rs4680)). *COMT* Val^{158} homozygotes have higher COMT activity and therefore lower brain DA and NE levels than Met^{158} homozygotes, with activity for heterozygotes falling in the middle (Chen et al., 2004). A considerable fraction of the variance in serotonin levels, on the other hand, is explained by $Val^{66}Met$ (rs6265) polymorphism of the gene coding for BDNF, which influences 5-HT receptor binding (Fisher et al., 2017) and the activity-dependent secretion of BDNF (Egan et al., 2003). In line with the importance of catecholaminergic and serotonergic neuromodulation in shaping brain circuit dynamics, genetic polymorphisms in *COMT* and *BDNF* have been established to influence cognition and behavior (Meyer-Lindenberg et al., 2005; Mier et al., 2010; Papenberg et al., 2020; Puig & Gulledge, 2011; Štrac et al., 2016; Tunbridge et al., 2019). Compelling evidence indicates that *COMT* $Val^{158}Met$ (rs4680) polymorphism is associated with modulation of neuronal activity in fMRI, especially in the prefrontal cortex (PFC) and with cognitive functions dependent on PFC (Meyer-Lindenberg et al., 2005; Mier et al., 2010; Papenberg et al., 2020; Robbins & Arnsten, 2009) while *BDNF* $Val^{66}Met$ polymorphism is implicated in in many aspects of behavior and cognition (Beste et al., 2010; Matsuo et al., 2009; Notaras et al., 2015). In addition to modulation 5-HT levels, activity-dependent

release of BDNF also influences the maintenance and formation of neuronal networks (Park & Poo, 2013; Zagrebelsky & Korte, 2014), thereby influencing cognition and behavior over lifetime. However, the influence of *COMT* Val^{158}Met and *BDNF* Val^{66}Met polymorphisms in neuronal circuit dynamics of fast neuronal oscillations identified with electrophysiological methods has remained uncharted.

We hypothesized here that neuromodulatory drive could influence large-scale oscillation dynamics. Genome-wide association (GWAS) studies have demonstrated the clinical relevance of genes on functional and structural MRI data (Pereira et al., 2018) and for oscillatory activity in the brain using EEG (Smit et al., 2018). However, given the huge (N > 1000) sample size required for GWAS analysis, which is not feasible for MEG studies, and due to the lack of polygenic risk scores for oscillation dynamics, we focused on polymorphism in *COMT* Val^{158}Met and *BDNF* Val^{66}Met candidate genes, which have been already and repeatedly associated with modulations of neuronal dynamics in fMRI and with variability in cognitive performance (Hariri et al., 2003; Meyer-Lindenberg et al., 2005; Mier et al., 2010; Papenberg et al., 2020; Tunbridge et al., 2019). We hypothesized that *COMT* Val^{158}Met and *BDNF* Val^{66}Met could influence oscillation amplitudes, phase synchronization, and their LRTCs and contribute to the large inter-individual variability therein. Importantly, brain criticality is primarily thought to be controlled by the excitation-inhibition (E/I) ratio so that critical dynamics emerge at balanced E/I while excess of inhibition or excitation leads to sub- or super-critical dynamics, respectively (Plenz & Thiagarajan, 2007; Poil et al., 2012; Shew et al., 2009). We thus further hypothesized that neuromodulation could influence oscillation dynamics via modulating critical dynamics in the brain.

To test these hypotheses, we measured resting-state brain dynamics with MEG and estimated local oscillation amplitudes, large-scale phase synchronization, and LRTCs from individually source-reconstructed MEG data. We then investigated their correlation with the *COMT*

Val[158]Met and *BDNF* Val[66]Met polymorphisms estimated from SNP analysis (Fig 1) and compared the results with predictions from computational modeling. In line with the predictions of the brain criticality framework and computational modeling, we found that the *COMT* Val[158]Met and *BDNF* Val[66]Met polymorphisms influenced local oscillation amplitudes and LRTCs, while *BDNF* Val[66]Met polymorphism also influenced the strength of large-scale synchronization.

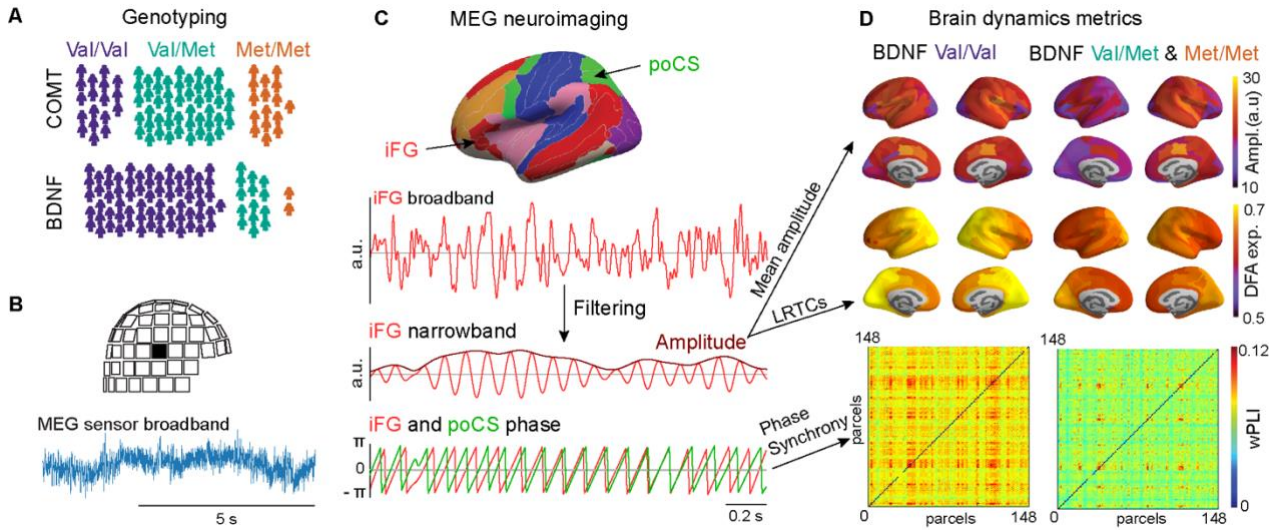

Fig 1. A schematic of study outline and rationale.
(A) Genotyping of the participants (N = 82) was used to identify the *COMT* Val[158]Met (rs4680) and *BNDF* Val[66]Met (rs6265) genetic polymorphisms. (B) Broadband MEG data were recorded from each participant with 306-channel MEG during ~8-minute resting state. (C) MEG data were source-reconstructed using minimum-norm estimation with individual MRI-based head and cortical surface anatomy and collapsed to cortical parcels (upper panel). Parcel-wise broadband signals (shown for inferior frontal gyrus, iFG, in 2nd panel) were filtered to narrowband signals (signal and amplitude envelope (shown here for the iFG in 3rd panel). From the narrowband signal, instantaneous phase was extracted (shown for iFG and posterior central sulcus, poSC, in lower panel). Mean amplitudes and LRTCs were estimated for each parcel from amplitude envelope time series, and inter-parcel phase synchronization for all parcel pairs from phase time series. (D) In group analyses, we assessed the anatomical distribution of mean amplitudes, LRTCs, and synchronization within the polymorphism groups and identified statistically significant differences between these groups (Figs 2-4).

Results

COMT Val/Met and *BDNF* Val polymorphisms are associated with the strongest oscillation amplitudes

To characterize local synchronization, we first evaluated mean oscillation amplitudes for 26 wavelet frequencies between 3–60 Hz and averaged the mean amplitudes across 148 cortical parcels separately for participants grouped according to the *COMT* Val^{158}Met (Val/Val, Val/Met, Met/Met) and the *BDNF* Val^{66}Met (Val/Val and the combined Val/Met and Met/Met) polymorphisms. As observed commonly in resting state, oscillation amplitudes peaked in the alpha band (α, 8–14 Hz) (Fig 2A). We then clustered oscillations to frequency bands based on the similarity of the anatomical amplitude maps using Louvain clustering (Fig S1) that revealed spatial similarity in theta (θ, 3–7 Hz), alpha, beta (β, 14–30 Hz) and gamma (γ, 30–60 Hz) frequency bands. Statistical analysis for these frequency bands using repeated measures ANOVA demonstrated a main effect of frequency [$F(1.86, 150.76) = 98.54$, $p = 6.47\text{E-}27$, $\eta_p^2 = 0.549$] ($N = 82$) on oscillation amplitudes at the whole-brain level. Post-hoc tests indicated that the oscillation amplitudes were stronger in the α band than in the θ ($t(81) = 14.14$, $p = 8.93\text{E-}23$), β ($t(81) = 2.75$, $p = 0.043$), and γ ($t(81) = 5.11$, $p = 1.3\text{E-}5$) bands (t-test, Bonferroni corrected). β-band amplitudes were also stronger than in θ ($t(81) = 15.71$, $p = 1.57\text{E-}25$) and γ ($t(81) = 5.49$, $p = 3.0\text{E-}6$) bands, and γ amplitudes were stronger than θ band amplitudes ($t(81) = 12.73$, $p = 2.75\text{E-}20$). Using univariate ANOVAs that controlled for age effects, we also showed both in the wavelet frequencies (Fig 2A) and in the canonical frequency bands (Fig S2) that *COMT* Val^{158}Met and *BDNF* Val^{66}Met polymorphisms had no impact on oscillation amplitudes at the whole-brain level. We further confirmed that age or the percentage of female and male participants did not differ between the polymorphism groups (Tables S1 and S2).

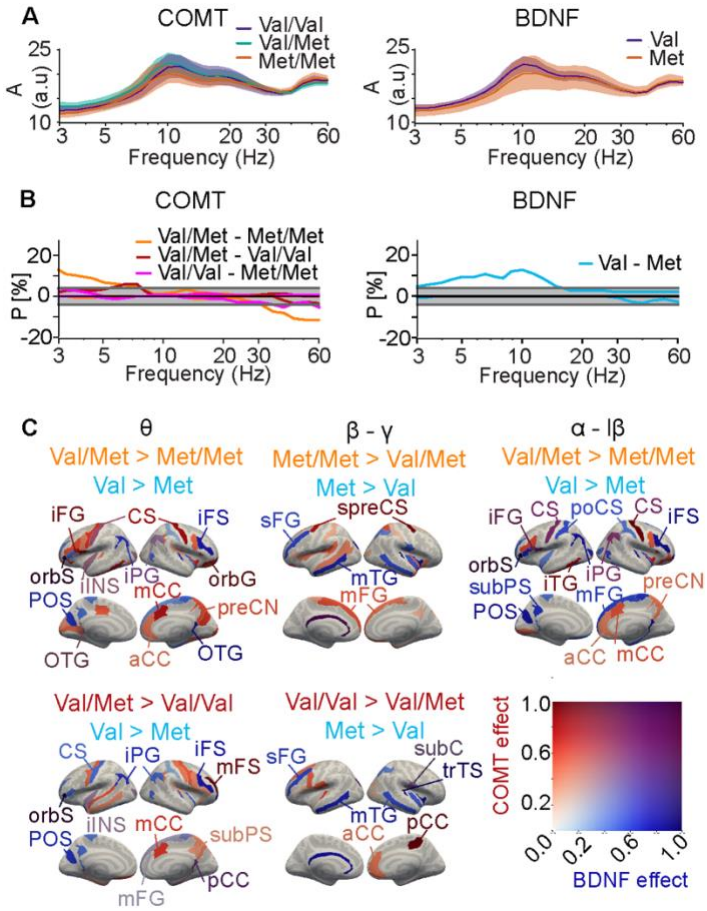

Fig 2. *COMT* and *BDNF* polymorphisms influence oscillation amplitudes.
(A) Oscillation amplitudes averaged across parcels for the *COMT* (Val/Val, purple, n = 18; Val/Met, turquoise; n = 48; and Met/Met, orange, n = 16) and *BDNF* polymorphism groups (Val/Val, purple, n = 66; Met carriers, orange, n = 16). Shaded areas represent 95% bootstrapped confidence intervals of the group means. (B) The fraction P of parcels with a significant positive and negative pairwise difference (shown separately) between the *COMT* and *BDNF* polymorphisms groups in oscillation amplitudes (Mann–Whitney-U test, $p < 0.05$). The light grey area indicates the 5% alpha level for findings expected by chance under the null hypothesis and the dark grey area indicates the range (3% total) in fractions of significant parcels observable by chance at $p_q < 0.05$ in any single frequency band across the spectrum (26 frequencies). (C) Cortical parcels where the amplitudes differed significantly between polymorphism groups (indicated above the brain surfaces) in the θ (3–7 Hz), β–γ (20–60 Hz), and α to low-β (7–18 Hz) frequency ranges in at least one of the individual frequencies. The color scale indicates the max-normalized amplitude differences for *COMT* (red) and *BDNF* (blue) polymorphisms independently, so that parcels where the effects are co-localized have purple hues. Abbreviations are formed from a combination of i) Areas: a = anterior, ca= calcarine, d = dorsal, i = inferior, la = lateral, m = middle, mrg = marginal, opc = opercular, p = posterior, s = superior, tr = triangular and ii) Lobes: C= central / cingulate, F = frontal, P = parietal, O = occipital, T = temporal, and iii) G = Gyrus, S = Sulcus. Additional abbreviations: subC = subcentral gyrus/sulcus, preCN=precuneus.

To identify possible anatomically limited polymorphism effects, we tested significant pairwise differences between polymorphism groups at the anatomical resolution of individual parcels and for each frequency. For *COMT*, the amplitudes were stronger (Mann-Whitney-U test, $p < 0.05$) for Val/Met heterozygotes than for either Met or Val homozygotes in the θ band (3–7 Hz) (in up to 13% and 6% of cortical parcels, respectively) (Fig 2B), whereas in the high-β to γ (20–60 Hz) bands, amplitudes were larger for Met homozygotes (12% of parcels compared to Val/Met, 6% compared to Val/Val). For *BDNF*, oscillation amplitudes were stronger for the Val homozygotes than for the Met carriers in the θ and in the α to low-β bands (up to 13% of parcels). We next plotted the amplitudes in each cortical parcel separately for each polymorphism group (Figs S3-S4) and their significant differences (Fig 2C) in the cortical anatomy. Stronger oscillation amplitudes for the *COMT* Val/Met heterozygotes were localized to the central sulcus (CS), anterior, mid- and posterior cingulate cortex (aCC, mCC, pCC), inferior frontal gyrus (iFG), right-hemispheric middle frontal gyrus (mFG) and inferior parietal gyrus (iPG), inferior part of the insula (iINS) and precuneus (preCN) (Fig 2C). The parcels were co-localized with fMRI-based functional parcellation (Fig S5), which revealed that these parcels mostly belonged to the frontoparietal network (FPN) and default mode network (DMN). Of these regions, iPG and left iINS and left CS showed also larger amplitudes for *BDNF* Val homozygotes than for Met carriers. However, the larger amplitudes for *COMT* Met homozygotes compared to Val/Met heterozygotes in the β-γ bands were localized to superior precentral sulcus (spreCS), corresponding to frontal eye fields (FEF). For *BDNF* Val homozygotes, oscillation amplitudes were larger than in Met carriers in iFS, parieto-occipital sulcus (POS) and postcentral sulcus (poCS) in θ to low-β bands. *COMT* and *BDNF* jointly affected the θ and the α to low-β band oscillation amplitudes in the CS and iPG. In the high-β to γ bands, oscillation amplitudes were stronger for the *COMT* Val or Met homozygotes as compared to Val/Met heterozygotes in preCS, aCC, pCC and the middle frontal gyrus (mFG) and for the *BDNF*

Met carries as compared to *BDNF* Val homozygotes in the superior frontal gyrus (sFG) of the left hemisphere and middle temporal gyrus (mTG) of both hemispheres (Fig 2C). We further averaged amplitudes within the Yeo-parcellation (Yeo et al., 2011) that is functional systems parcellation (See Methods) derived from fMRI studies but found no evident patterns related to *COMT* nor *BDNF* polymorphism (Figs S5-S6).

COMT Val^{158}Met and *BDNF* Val^{66}Met polymorphisms influence DFA scaling exponents

We quantified long-range temporal correlations (LRTCs) in oscillation amplitude fluctuations by using detrended fluctuation analysis (DFA) (Hardstone et al., 2012) and estimated the mean DFA scaling exponents in all wavelet frequencies (3–60 Hz). To obtain a whole brain view on LRTCs, DFA exponents were first averaged across parcels separately for each *COMT* Val^{158}Met and *BDNF* Val^{66}Met polymorphism group for each frequency (Fig 3A). Statistical analysis for the canonical frequency bands with repeated measures ANOVA showed a main effect of frequency [$F(2.16, 174.70) = 123.65$, $p = 9.85\text{E-}36$, $\eta_p^2 = 0.604$] ($N = 82$). Post-hoc test indicated that DFA exponents in α band were stronger than in θ ($t(81) = 13.00$, $p = 1.00\text{E-}22$), β ($t(81) = 10.00$, p = 1.14E-11) and γ ($t(81) = 12.80$, $p = 3.58\text{E-}21$) bands (t-test, Bonferroni corrected). Similarly, also the β band DFA exponents were stronger than in θ ($t(81) = 10.33$, $p = 5.09\text{E-}14$) and γ ($t(81) = 10.75$, $p = 6.04\text{E-}17$) bands, and the DFA exponents in θ band were stronger than in γ band ($t(81) = 3.00$, $p = 0.008$). Univariate ANOVAs that controlled for age showed that *COMT* polymorphism had an effect on whole-brain DFA exponents in the γ frequency band averaged across the brain and within the canonical frequency band [$F(2, 75) = 3.80$, $p = .027$, $\eta_p^2 = 0.092$] ($n = 79$) (Fig 3A and S2). Group mean exponents were higher at the γ band for the *COMT* Val/Met individuals than for the Val/Val

($t(64) = 2.08$, $p = 0.043$, uncorrected) and Met/Met ($t(62) = 3.50$, $p = 0.001$) individuals when equal variances were not assumed. The *BDNF* polymorphism affected the whole-brain DFA exponents in the canonical α band [$F(1, 76) = 4.19$, $p = .044$, $\eta_p^2 = .052$], when age was controlled for ($n = 79$) (Fig S2), whereby the Val homozygotes exhibited larger LRTC exponents than the Met carriers (Fig 3A and S2).

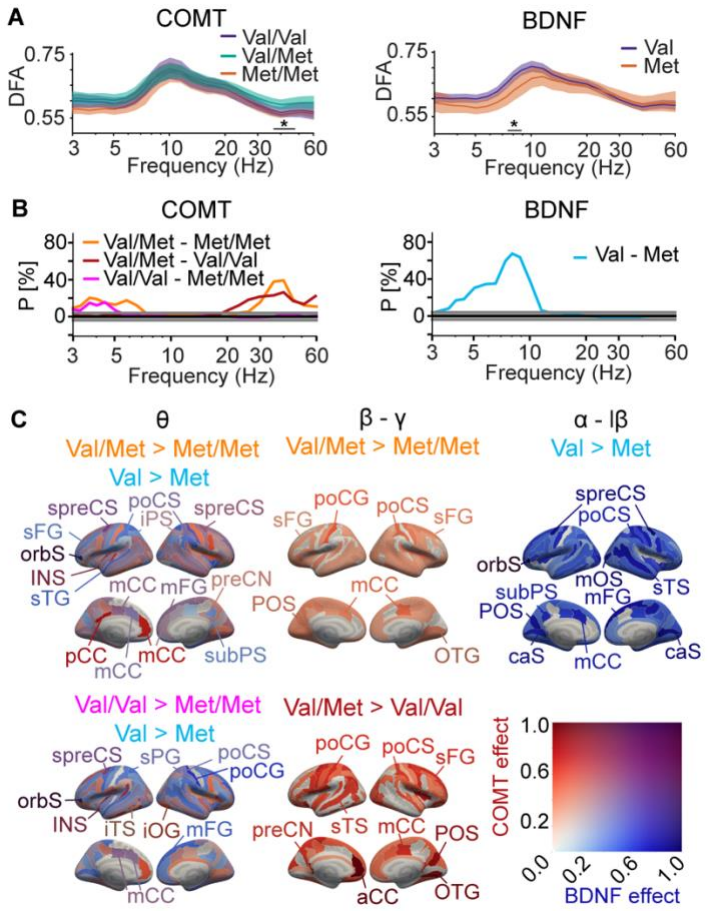

Fig 3. Influence of *COMT* and *BDNF* polymorphisms on LRTCs. (A) Detrended fluctuation analysis (DFA) exponents averaged across parcels for the *COMT* and *BDNF* polymorphism groups. Shaded areas represent 95% bootstrapped confidence intervals of group means. Black bar with asterisk denotes the range of frequencies with significant differences between the *COMT* and *BDNF* polymorphism groups (univariate ANOVA, with age as covariate, *: $p < 0.05$, uncorrected). (B) Fractions (P) of parcels with a significant positive and negative difference between C*OMT* and *BDNF* polymorphism groups in the DFA exponents (Mann–Whitney-U test, $p < 0.05$), as in Fig 2B. (C) Cortical areas where significant differences between polymorphism groups in the DFA exponents were found in the θ, β–γ and α– low-β bands (Mann–Whitney U test, $p < 0.05$, corrected). Colors and abbreviations as in Fig 2C.

Similar to oscillation amplitudes, *COMT* Val^{158}Met and *BDNF* Val^{66}Met polymorphisms had a more robust effect on the DFA exponents at the resolution of cortical parcels indicating large anatomical heterogeneity. DFA exponents were greater for the *COMT* Val/Met heterozygotes than for the Met homozygotes (Mann-Whitney-U test, $p < 0.05$) in the θ band (up to 20% of parcels) and in the β–γ band (up to 40%) (Fig 3B). Further, θ band DFA exponents were greater for Val/Val than for Met/Met (16%) and β–γ DFA exponents were greater in Val/Met than for Val/Val (26%) (Fig 3B). For *BDNF*, a very robust effect of polymorphism was found for DFA exponents. These were greater for Val homozygotes than Met carriers in the θ band (35%) and in α band (68%) (Fig 3B). The effect of *COMT* Val^{158}Met and *BDNF* Val^{66}Met on DFA exponents was thus more extensive compared to that found for oscillation amplitudes. The localization of DFA exponents for each polymorphism group (Figs S7-S8), and their significant differences (Mann-Whitney-U test, $p < 0.05$, Fig 3C) revealed wide-spread group differences. In the θ band, large differences between *COMT* Val/Met heterozygotes and Met homozygotes and between *BDNF* Val homozygotes and Met carriers were co-localized to preCS, mCC, and mFG (Fig 3C). DFA exponents in θ band were also greater for *COMT* Val/Met group in INS, pCC, and in β–γ band particularly in parcels of the somatomotor (SM) network, and DMN. *BDNF* Val homozygotes had greater α–low-β band LRTC exponents than Met carriers nearly in all parcels of the cortex (Fig 3C). Similar to oscillation amplitudes, no evident patterns were found in the Yeo-parcellation of functional systems (Fig S9).

Finally, to gain insight for the common effects of *COMT* Val^{158}Met and *BDNF* Val^{66}Met polymorphisms on oscillation amplitudes and DFA exponents, we co-localized their effects. This revealed co-localization in the parcels of PFC and PPC, CS and anterior cingulate structures (Fig S10). The effects of *COMT* and *BDNF* polymorphisms on LRCTs were widespread, in line with prior work and with the idea that LRTCs reflect global fluctuations in neuronal activity across the brain's modular structure (Monto et al., 2008; Palva et al., 2013; Zhigalov et al., 2017).

BDNF polymorphism correlates with the strength of large-scale phase-synchronization

To obtain a global view on the influence of *COMT* Val[158]Met and *BDNF* Val[66]Met polymorphisms on neuronal dynamics, we estimated their impact on inter-areal phase coupling of neuronal oscillations a.k.a. synchronization that constitutes a key characteristic of individual cortical dynamics and has fundamental influence on behavior (Brookes et al., 2011; Fell & Axmacher, 2011; Fries, 2015; Palva & Palva, 2012; Singer, 1999; Vidaurre et al., 2021). We estimated phase-synchrony among all cortical parcels with the weighted phase-lag index (wPLI) that is less sensitive to linear source mixing (Palva et al., 2018) and computed the mean synchronization for each of the *COMT* Val[158]Met and *BDNF* Val[66]Met polymorphism group (Fig 4A).

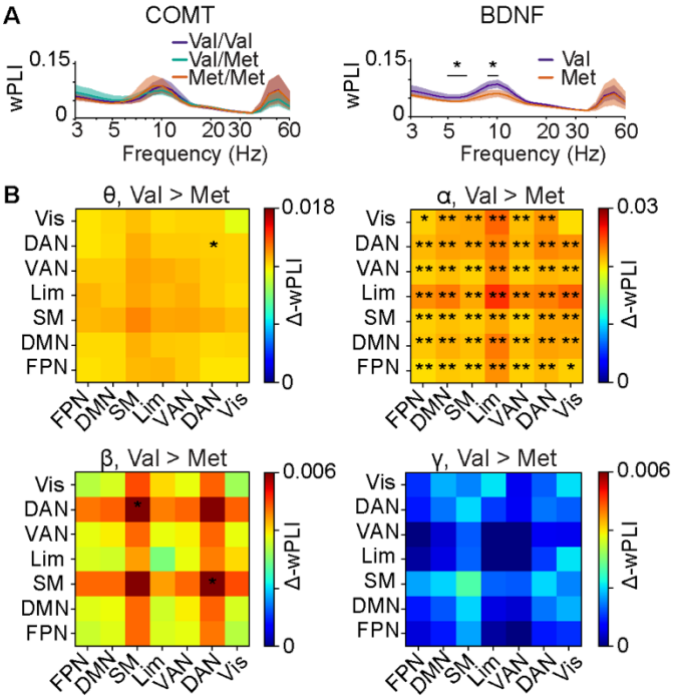

Fig 4. *BDNF* polymorphisms influence large-scale phase-synchronization. (A) Phase-synchronization averaged across the whole brain for the *COMT* Val[158]Met and *BDNF* Val[66]Met polymorphism groups with 95% bootstrapped confidence intervals. Black bars with asterisks denote the frequencies where a significant group difference was found (Kruskal-Wallis, *: $p < 0.05$, uncorrected). (B) The differences in the phase synchrony (Δ-wPLI) within and between functional

systems for the *BDNF* Val homozygotes and Met carries, averaged across hemispheres and wavelet frequencies in these frequency bands. Color indicates Δ-wPLI, red indicating stronger synchronization for *BDNF* Val^{66} homozygotes and blue for Met carriers. Stars denote the brain system pairs where the group difference was significant (Kruskal-Wallis, *: $p < 0.05$, uncorrected, **: $p < 0.01$, Benjamini-Hochberg corrected). Abbreviations: DAN = Dorsal attention network, DMN = Default Mode network, FPN = Frontoparietal network, Lim = Limbic system, SM= Somatomotor network, VAN = Ventral attention network, Vis = Visual network.

We did not find significant differences (Kruskal-Wallis test, $p < 0.05$) among the *COMT* Val^{158}Met polymorphism groups, but the mean synchronization for *BDNF* Val homozygotes was stronger than for *BDNF* Met carriers in the θ and α frequencies (Fig 4A). Taken that BDNF modulated oscillation amplitudes in much wider frequency range and because of robust synchronization in the alpha-band, these results are unlikely to be explained by increase in signal-to-noise ratio (SNR) in the narrow theta- and alpha-bands as show previously for cortex-wide synchronization networks (Palva et al., 2010; Siebenhühner et al., 2016).

To acquire neuroanatomical insight into the patterns of inter-areal synchronization in functional brain systems, we collapsed the parcel-wise synchronization estimates within brain systems defined by fMRI functional connectivity (Yeo et al., 2011) and for the same frequency bands that were used for estimating oscillation amplitudes and LRTCs (Fig S1). Corroborating the mean-synchronization result, synchronization between or within the subsystems did not differ significantly among the *COMT* Val^{158}Met polymorphisms (absolute values in Fig S11). However, *BDNF* Val homozygotes exhibited stronger synchronization than Met carriers in the α band between and within nearly all subsystems (Fig 4B and Fig S11, Kruskal-Wallis test, corrected with Benjamini-Hochberg). We also computed synchronization separately for each hemisphere and between the hemispheres. Interestingly, synchronization in the α and β bands was more robust for the left- and inter-hemispheric connections than for the right-hemispheric connections (Fig S12). Additionally, β-band synchronization was stronger for *BDNF* Val homozygotes than Met carriers

in the left-hemispheric attentional networks including FPN, dorsal attention network (DAN), ventral attention (VAN) and Limbic networks (Lim) and DMN.

Computational model-based approach to neuromodulation effects on critical synchronization dynamics.

We hypothesized that at the level of macroscopic brain dynamics, the effects of *COMT* Val^{158}Met and *BDNF* Val^{66}Met polymorphisms could be addressed in the context of brain criticality if these polymorphisms bias the underlying "control parameter" that tunes the distance of neuronal systems to criticality. This control parameter is assumed to be the gross excitation / inhibition (E/I) ratio that arises from the functional net effects of inhibitory and excitatory synaptic, cellular, biophysical, and microcircuit mechanisms at the systems-level (Deco et al., 2021). Brains are thought to normally operate in a slightly subcritical regime (Priesemann et al., 2014), where LRTCs in human brain activity (Linkenkaer-Hansen et al., 2001; Palva et al., 2013; Smit et al., 2013; Zhigalov et al., 2015) exhibit large inter-individual variability. In the brain criticality framework, the carriers of different variants of the *COMT* Val^{158}Met and *BDNF* Val^{66}Met polymorphisms would therefore be located closer to or further away from the critical point. This would lead to the different genotype cohorts showing consistent differences in local amplitudes, global synchronization, and LRTCs.

To assess the relationships of the observable brain dynamics measures with the control parameter, we used a computational model of synchronization dynamics exhibiting a transition from sub- to super-critical dynamics (Fig 5A). We implemented a nested Kuramoto model with separable local network (cortical parcel) and large-scale (whole-brain network) levels (Siebenhühner et al., 2020). Synchronization here was regulated by local and global coupling parameters that simulate the E/I balance (or neural gain) that is the likely primary control parameter

for brain criticality (Shew et al., 2009; Stephani et al., 2020). In the model, increasing coupling led to parallel strengthening of local amplitudes, large-scale synchronization, and LRTCs throughout the subcritical regime up to the critical point (Fig 5A). We set all oscillators' frequencies to a constant value (10 Hz) and predicted the synchronization dynamics of neuronal oscillations for two hypothetical cohorts (A, control parameter from 8.25 to 9.25; and B, control parameter from 8.75 to 9.75) operating in a subcritical regime. The model predicted that the cohort B, operating at greater excitability / gain, would exhibit larger oscillation amplitudes, LRTCs, and large-scale synchronization (Fig 5A-B), and as a novel model-predicted measure, larger mutual correlations (Fig 5C) between these three values.

To next investigate whether *COMT* and *BDNF* polymorphisms could influence synchronization dynamics via these mechanisms, we computed these dynamics separately for different polymorphism groups for the frequency bands in which we found the main effects of *COMT* and *BDNF* polymorphism. In line with the model predictions, the elevated θ-band amplitudes and LRTC exponents in *COMT* Val/Met group (Fig 5D) were paralleled with stronger correlation of local oscillation amplitudes and LRTC exponents (Fig 5E, Val/Met > Met/Met 95% and Val/Met > Val/Val in 84% of permutations). Similarly, for the *BDNF*, elevated θ-band amplitudes and LRTCs in Val homozygotes (Fig 5F) were associated with stronger correlation of local oscillation amplitudes and LRTCs (Fig 5G, Val > Met in 92% of permutations, for γ bands see Fig S13). In contrast, the elevated α-band global synchronization in *BDNF* Val/Val group (Fig 5F) was not associated with elevated correlation with LRTCs (Fig 5G). These findings thus provide converging evidence that locally, *COMT* $Val^{158}Met$ and *BDNF* $Val^{66}Met$ polymorphisms impact oscillation dynamics as predicted by the framework of brain criticality under the hypothesis that these polymorphisms influence the control parameter of cortical critical dynamics. In contrast, the most robust effects of *BDNF* on large-scale synchronization were not in line of the model

predictions, suggesting that these were mediated mainly by other factors than the control parameter of brain criticality.

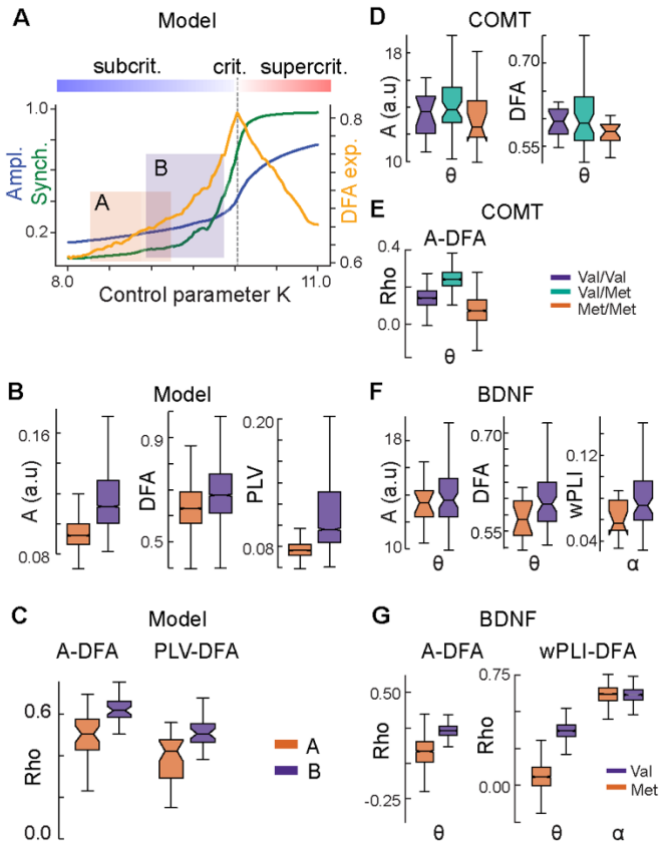

Fig 5. Model and experimental evidence for modulation of brain criticality. (A) Computational model of local and inter-areal synchronization dynamics in the realistic human connectome shows that both local amplitude (blue) and inter-areal synchronization (green) increase monotonically with increasing coupling (control parameter K) and exhibit a phase-transition between low- (subcritical) and high-synchronization (supercritical) regimes. Conversely, the DFA scaling exponent (yellow), a measure of long-range temporal correlations (LRTCs), peaks at the critical point. The model predicts that two cohorts (A, B) with subjects operating in different parts of the subcritical regime should exhibit group differences in amplitude, LRTCs, and inter-areal synchronization. (B) Local amplitude (A), DFA exponents, and inter-areal phase synchronization (PLV) in modeled data for two cohorts A (orange) and B (purple). All metrics are greater for the cohort B that is designed to operate closer to the critical point (see panel A) than cohort A. The box ends indicate the lower quartile (Q1, 25th percentile) and upper quartile (Q3, 75th percentile) across cortical regions/parcels, notches indicate the median, and whiskers indicate the range of Q1 – 1.5 * IQR and Q3 + 1.5 * IQR, where IQR is the inter-quartile range (Q3-Q1). (C) Correlations between amplitude and DFA exponents, and between PLV and DFA, in modeled data are also larger for cohort B than the more subcritical cohort A. (D) A and DFA exponents for *COMT* Val^{158}Met polymorphism groups in the θ band in MEG data. (E) Correlation between A and DFA exponents in θ band differs between *COMT* Val^{158}Met polymorphism groups. (F) A and DFA exponents in θ band, and global phase synchronization (wPLI) in α band for the *BDNF* polymorphism groups in

MEG data. (G) Correlation between A and DFA exponents differs between *BDNF* Val^{66}Met polymorphism groups in the θ-band, as does the correlation between wPLI and DFA exponents in θ, but not in α band.

Discussion

Inter-individual variability in spontaneous brain dynamics shapes human behavioral performance and cognitive ability (Donhauser & Baillet, 2020; Palva & Palva, 2012; Palva & Palva, 2018; Siebenhühner et al., 2020; Vidaurre et al., 2021). While the causes of this variability are diverse, genetics influences numerous factors that are important for brain oscillation dynamics on multiple scales observed in human MEG and EEG data (Leppäaho et al., 2019; Linkenkaer-Hansen et al., 2007; Van Pelt et al., 2012). Macroscopic oscillations can be influenced through regulation of neural circuits and dynamic circuit motifs on a cellular level (Leppäaho et al., 2019; Van Pelt et al., 2012; Womelsdorf et al., 2014) as well as coupling of metabolic activity and connectivity (Hahn et al., 2020). However, it is not well understood how the genetic biases of molecular, cellular, and micro-circuit mechanisms translate into alterations of macroscopic brain dynamics that are observable in electrophysiological neuroimaging. We tested here the hypothesis that the *COMT* Val^{158}Met and *BDNF* Val^{66}Met genetic polymorphisms contribute to the variability in emergent local (oscillation amplitudes and LRTCs) and global (inter-areal phase synchronization) dynamics of neuronal oscillations. We showed that both *COMT* and *BDNF* polymorphisms influenced oscillation amplitudes and LRTCs, while the *BDNF* polymorphism also impacted the strength of global synchronization. Using computational modelling, we furthermore showed that the influence of *COMT* and *BDNF* on local oscillation dynamics could be achieved via modulations of the brain E/I balance in line with the established role of *COMT* and *BDNF* in the regulation of neuronal activity via DA, NE, and 5-HT.

Local oscillation strength and dynamics are modulated by genetic polymorphism in *COMT* and *BDNF*

The amplitude of θ oscillations was greater for *COMT* Val/Met heterozygotes than for *COMT* Val homozygotes, and the amplitudes of θ and α oscillations were greater for *BDNF* Val homozygotes than for Met carriers. These data thus add to scarce prior observations about *COMT* polymorphism effects on electrophysiological activity (Bodenmann et al., 2009; Bonetti et al., 2021; Garcia-Garcia et al., 2017), which have shown, using EEG sensor level analysis, that *COMT* Val homozygotes had lower individual α power in both waking state and sleep than Met homozygotes (Bodenmann et al., 2009) and that the *COMT* polymorphism influences phase-resetting of γ oscillatory activity in attention (Garcia-Garcia et al., 2017). Our results provide strong evidence for *COMT* polymorphism influencing local amplitude dynamics in widespread brain areas and frequency ranges. We furthermore found the *BDNF* Val homozygotes to exhibit stronger α band amplitudes bilaterally in frontoparietal regions and parcels of the visual system. These results are in line with previous research (Chen et al., 2016) and findings that 5-HT plays a critical role in modulating cortical activity and neuronal oscillations (Gener et al., 2019; Puig & Gulledge, 2011).

To our knowledge, this study is the first to report the influence of genetic polymorphism on LRTCs in oscillation amplitude fluctuations. LRTCs were stronger for the *COMT* Val/Met heterozygotes than for Val or Met homozygotes in θ and γ bands and stronger for *BDNF* Val homozygotes than for Met carriers in α- low-β bands, demonstrating that near-critical dynamics of brain oscillations is influenced by *COMT* and *BDNF* polymorphisms. The temporally widespread effects of *COMT* and *BDNF* polymorphisms on both instantaneous amplitudes and their LRTCs could putatively stem from *COMT* influencing both phasic and tonic firing modes of DA neuronal

spiking (Wiencke et al., 2020) and/or from multi-scale cortical ensemble codes regulated by NE (Totah et al., 2019).

As *COMT* Val/Met heterozygotes have intermediate COMT activity, and therefore intermediate brain DA and NE levels compared to Val and Met homozygotes (Chen et al., 2004) and as operating near criticality has been associated with optimal processing capacity and flexibility among possible states (Beggs, 2008; Chialvo, 2010; Deco & Jirsa, 2012), the finding of the largest θ and γ band LRTC exponents in the *COMT* Val/Met polymorphism group, is consistent with previous findings showing that the impact of neuromodulation on cognition follows an "inverted-U-shaped" function. According to these findings both excessively low and excessively high neuromodulation impairs performance (Cools & D'Esposito, 2011; Farrell et al., 2012; Harris & Thiele, 2011; Meyer-Lindenberg et al., 2005; Papenberg et al., 2020; Vijayraghavan et al., 2007). The association between *COMT* Val^{158}Met polymorphism and neuronal activity has been frequently observed in fMRI to be predominantly localized to PFC (Meyer-Lindenberg et al., 2005; Mier et al., 2010; Papenberg et al., 2020; Robbins & Arnsten, 2009), which has low DA reuptake and higher COMT levels. In our data, the influence of *COMT* Val^{158}Met polymorphism on instantaneous amplitudes was not localized specifically to PFC, but to multiple specific cortical regions in the FPN and cingulo-opercular (CO) networks. These networks underlie the dual control of executive functions (Dosenbach et al., 2008) and have been shown to be functionally coupled also in the resting state (Newbold et al., 2021) which is in agreement with the role of DA in cognitive control (Cools & D'Esposito, 2011; Ott & Nieder, 2019). Further, our results are in line with brain-wide distribution of catecholamine-induced changes in DA and NE in intrinsic fMRI correlations (van den Brink et al., 2018) and with findings that DA innervation covers the entire cortex (Björklund & Dunnett, 2007) and that Locus Coeruleus' NE projections reach a variety of targets (Totah et al.,

2019). Overall, these results support the idea that via DA and NE *COMT* influences local oscillation dynamics in a variety of cortical regions important for cognition.

Polymorphism in *BDNF* but not in *COMT* influences inter-areal synchronization dynamics

We found that *BDNF* Val^{66}Met but not *COMT* Val^{158}Met polymorphism influenced large-scale global inter-areal phase synchronization. This effect was robust in the α band, in which stronger synchronization was observed for *BDNF* Val homozygotes in all functional subsystems except within the visual system. *BDNF* Val homozygotes also had stronger θ synchronization within DAN and stronger β synchronization between DAN and SM networks and between the frontoparietal attention networks and DMN but only in the left hemisphere. This robust modulation of synchronization dynamics by *BDNF* polymorphism could contribute to significant differences across individuals in behavior and cognition, which have been shown to be strongly influenced by spatial and spectral characteristics of oscillatory synchronization (Betti et al., 2018; Mostame & Sadaghiani, 2020; Siebenhühner et al., 2020).

However, large-scale synchronization was not influenced by *COMT* Val^{158}Met polymorphism. This suggests that *COMT* polymorphism does not play a significant role in shaping instantaneous resting-state network synchronization even though it modulates local oscillatory dynamics in both sub-second and seconds-to-minutes timescales and despite catecholamines being related to fMRI-based changes in functional connectivity (van den Brink et al., 2018). These differences might be explained by different effects of catecholaminergic levels on BOLD signal and electrophysiological connectivity or by *COMT* polymorphism having more subtle effects on neuronal dynamics compared to neuropharmacological interventions.

Computational modelling predicts local *COMT* and *BDNF* influences to depend on net excitability

Near-critical synchronization dynamics has been proposed as a fundamental operating principle of brain functioning, enabling transient and flexible computations that are beneficial for the individual by maximizing information storage and transmission (Cocchi et al., 2017; Daffertshofer et al., 2018; Deco & Jirsa, 2012; Kinouchi & Copelli, 2006; Palva & Palva, 2018; Priesemann et al., 2014; Shew & Plenz, 2013). This notion has been supported experimentally by behavioral data (Simola et al., 2017) and *in vitro* studies (Shew et al., 2009). Here we show that genetic polymorphisms in *COMT* and *BDNF* influenced the individual near-critical synchronization dynamics and proximity to the critical point.

The systems-level E/I ratio (or gain) is thought to be the primary control parameter for the regulation of critical brain dynamics (Shew et al., 2009; Stephani et al., 2020), and has been shown to influence brain dynamics in whole-brain modeling (Schirner et al., 2018). We postulated that the observed differences in neuronal synchronization dynamics are due to neuromodulation-related shifts in the system's net E/I ratio. Comparison of the experimental and computational-model data showed that the *COMT* Val^{158}Met and *BDNF* Val^{66}Met polymorphisms influenced local oscillatory dynamics and their correlations in the θ band in line with the brain criticality framework. More specifically, *COMT* Val^{158}Met heterozygotes and *BDNF* Val^{66} homozygotes had greater amplitudes and LRTCs and stronger correlations between LRTCs and oscillation amplitudes than the other polymorphism groups in θ band, indicating that they are associated with a higher value of the underlying control parameter, *i.e.*, with greater net excitatory drive or neuronal gain (Ferguson & Cardin, 2020) compared to *COMT* ^{158} homozygotes and *BDNF*^{66} Met carriers. This is in accordance

with the framework in which neuromodulatory drive influence brain-state energy landscape facilitating with transitions in the whole-brain neural states (Braun et al., 2021; Munn et al., 2021).

In contrast, we found no evidence for that the influence of *BDNF* Val^{66}Met polymorphism on global α-band synchronization could be explained within the brain criticality framework. This finding implies that the strongest effects of *BDNF* polymorphisms on global synchronization might not be due to a shift in global excitation, but to other mechanisms such as the influence of BDNF on maintenance, maturation, and formation of neuronal networks (Park & Poo, 2013; Zagrebelsky & Korte, 2014) putatively via receptor TrkB (neurotrophic receptor tyrosine kinase 2) signaling (Castrén & Monteggia, 2021; Winkel et al., 2021). These could impact large-scale network synchronization via changes in structural connectivity (Mostame & Sadaghiani, 2020) or via changes in brain gray matter whose density has been shown to be associated with neuroreceptor and neurotransporter availabilities (Manninen et al., 2021) and whose thickness is associated with the structure of oscillatory networks (Mahjoory et al., 2020).

Conclusions

Our data showed that the *COMT* Val^{158}Met and *BDNF* Val^{66}Met polymorphisms contribute to the variability of oscillation dynamics, their LRTCs, and synchronization dynamics and adds on to the scarce data on the genetic basis of oscillatory neuronal dynamics. In addition to *COMT* and *BDNF*, many other genetic factors are likely to contribute to oscillation dynamics, as observed for the cortical structure (Grasby et al., 2020), but this remains to be charted in future studies.

Because oscillation amplitudes, LRTCs, and global synchronization dynamics are predictive of behavioral variability over both long (Palva et al., 2013; Smit et al., 2013) and sub-second time scales (Palva & Palva, 2012), *COMT* Val^{158}Met and *BDNF* Val^{66}Met polymorphisms may underlie individual differences in trait-like behavior and cognitive performance via their effect on critical

oscillatory dynamics and synchronization. Differences in these dynamics caused by genetic polymorphisms are likely to influence individuals' cognitive and mental development and may predispose them to specific brain diseases. In line with the latter idea, alterations in the brain E/I ratio have been suggested to predispose individuals to dementia and Alzheimer's disease (Pusil et al., 2019). Our results thus point in new directions for the investigation of how genetic factors could translate to behavioral variability via modulations of the systems-level neuronal dynamics.

Materials and methods

Participants and data acquisition

Resting-state brain activity was recorded from healthy volunteers (*N* = 82, 18–55 years of age; mean age: 29 years; 6 left-handed; 44 female) with 306-channel MEG (Vectorview, Elekta-Neuromag, LtD) at a sampling rate of 600 Hz. The subjects fixated on a central fixation cross throughout the ~8 min resting-state MEG-recording (duration 7.8 ± 2.9 min, mean ± standard deviation, Tables S1 and S2). Blood samples for the collection of DNA were obtained before each MEG session. T1-weighted anatomical magnetic resonance imaging (MRI) MP-RAGE scans were obtained for each participant at a resolution of 1 × 1 × 1 mm using a 1.5 T MRI scanner (Siemens, Germany) on a separate day. The dataset collected for this study is part of a broader project "Tunteet" that includes also other datasets and paradigms. The study was performed in accordance with the Declaration of Helsinki and with permission of the Ethical Committee of the Helsinki University Central Hospital. All participants gave a written informed consent prior to the recordings.

Genotyping

DNA was extracted from blood samples according to standard procedures at the National Institute for Health and Welfare. DNA samples were genotyped at Estonian Genome Center using Infinium PsychArray-24 v1.1 (Illumina). Quality control (QC) was performed with PLINK 1.9 (www.cog-genomics.org/plink/1.9/) (Chang et al., 2015). Markers were removed for missingness (> 5%) and Hardy-Weinberg equilibrium ($p < 1 \times 10^{-6}$). Individuals were checked for missing genotypes (> 5%), relatedness (identical by descent calculation, PI_HAT > 0.2) and population stratification (multidimensional scaling). Our sample for the *COMT* gene consisted of 18 Val/Val, 48 Val/Met, and 16 Met/Met individuals (Table S1). A one-way ANOVA confirmed that the *COMT* polymorphism groups did not differ in terms of age [$F(2, 46) = 0.05$, $p = .984$] and the duration of the resting state recording [$F(2, 46) = 0.32$, $p = .726$]. A chi-square test further confirmed that the percentages of female and male participants did not differ between the *COMT* polymorphism groups [$X^2(2) = 2.11$, $p = .349$]. The *BDNF* sample consisted of 66 Val/Val, 14 Val/Met, and 2 Met/Met individuals (S2 Table). As the Met/Met polymorphism had a low frequency, we combined Met carriers (*i.e.*, Val/Met and Met/Met polymorphisms) into one group (see also Beste et al., 2010). An independent samples *t*-test (2-tailed) confirmed that the *BDNF* polymorphisms did not differ in terms of age [$t(32) = 0.20$, $p = .847$] or the length of the resting state recording [$t(32) = 0.76$, $p = .444$]. A chi-square test showed no differences in the percentages of female and male participants between the *BDNF* polymorphisms [$X^2(1) = 0.00$, $p = .995$].

Preprocessing and filtering of MEG data

Signal space separation method (tSSS) (Taulu et al., 2005) with the Maxfilter software (Elekta Neuromag, Helsinki, Finland) was used first to suppress extracranial noise, interpolate bad channels and to co-localize the recordings in signal space individually for each participant. Next, independent

component analysis (ICA, Matlab toolbox Fieldtrip (Oostenveld et al., 2011) was used to extract and exclude signal components that were correlated with eye movement, blink and cardiac artifacts. The preprocessed MEG data were filtered into 26 logarithmically spaced frequency bands, f_{min} = 3 Hz; f_{max} = 60 Hz, using complex Morlet Wavelets

$$w(t, f_0) = A\exp(-t^2/2\sigma_t^2 2)\exp(2i\pi f_0 t),$$

where $\sigma_t = m/2\pi f_0$, i is the imaginary unit, m (=5) defines the compromise between time and frequency resolution, and f_0 is the center frequency. After filtering, the time-series data were decimated to a frequency-dependent sampling rate of between 2 and 5 times the center frequency.

Source Analysis and Surface Parcellations

Volumetric segmentation of the MRI data, surface reconstruction, flattening, cortical parcellations and neuroanatomical labeling with the Freesurfer/Destrieux atlas (Destrieux et al., 2011) were performed using FreeSurfer software (http://surfer.nmr.mgh.harvard.edu/). Single-layer boundary element conductivity models and cortically constrained source models for the MEG-MRI co-localization and the preparation of the forward and inverse operators (Dale et al., 2000) were carried out using minimum norm estimate with MNE software (https://mne.tools/stable/index.html) (Gramfort et al., 2014). Noise covariance matrices (NCMs) were computed using preprocessed broad-band filtered (125–195 Hz, with 150 Hz notch) MEG time series around synthetic resting state events that were spaced in every 1 seconds and then used to compute minimum-norm estimate (MNE) inverse operators for all wavelet frequencies as previously (see Siebenhühner et al., 2020). These inverse operators were used to project the sensor-space data into source-space. The source models had dipole orientations fixed to the pial surface normal and a 5 mm inter-dipole separation

through the cortex, which yielded models containing 5000–8000 source vertices per hemisphere. As in previous studies (Korhonen et al., 2014; Siebenhühner et al., 2020), source-vertex time-series were then collapsed into parcel time series with an individually source-reconstruction-accuracy-(fidelity-) optimized collapse operators. We used a 400-parcel parcellation that was obtained by iteratively splitting the largest parcels of the Destrieux atlas (148 parcels) (Destrieux et al., 2011) along their most elongated axis using the same parcel-wise splits for all participants. Parcels were also assigned to functional systems based on Yeo's 7-parcel scheme derived from fMRI-connectivity (Yeo et al., 2011). To control for source-reconstruction accuracy, we estimated *parcel fidelity* as a measure of source-reconstruction accuracy (Korhonen et al., 2014).

Estimation of oscillation amplitudes and long-range temporal correlations

The parcel-wise narrow-band filtered time-series were used for cortex-wide mapping of induced oscillation amplitudes (A), LRTCs in oscillation amplitude envelopes, as well as for mapping cortex-wide phase-synchronization networks. Data were averaged for each cortical parcel and frequency separately for subjects in each *COMT* and *BDNF* polymorphisms group. The LRTC exponents of the amplitude envelopes were quantified with detrended fluctuation analysis (DFA) (Hardstone et al., 2012).

DFA was applied in two stages. First, time series *X(k)* were normalized to zero mean and the cumulative sum of the signal was computed:

$$y(k) = \sum_{i=1}^{k} [X(i) - \langle X \rangle]$$

The integrated signal *y(k)* was then segmented into multiple time windows Δt from 1 to 100 s with minimum window length of 20 cycles and maximum of 100 (length multiplier 1.2) (Linkenkaer-

Hansen et al., 2001). Second, each segment of integrated data was locally fitted to a linear function $y_{\Delta t}(k)$ and the mean-squared residual $F(\Delta t)$ was computed:

$$\sqrt{\frac{1}{N}\sum_{k=1}^{N}[y(k) - y_{\Delta t}(k)]^2}$$

where N is the total number of data points.

The power law scaling exponent β was defined as the slope of linear regression of the function $F(\Delta t)$ plotted in log–log coordinates, estimated using a least-squares algorithm. The scaling exponent β can be considered a measure of temporal clustering so that $0.5 < \beta < 1.0$ indicates power-law scaling behavior and the presence of temporal correlations, whereas values around 0.5 indicate uncorrelated noise.

Analysis of inter-areal synchronization

To estimate cortex-wide synchronization connectomes, we computed for each subject and for each frequency, phase synchronization between all 400 parcels (or parcels within the left or right hemisphere) using the weighted phase-lag index (wPLI) (Vinck et al., 2011) which is defined as

$$wPLI_{a,b} = \frac{|E\{im(X_{ab})\}|}{E\{|im(X_{ab})|\}} = \frac{\left|E\left\{|im(X_{ab})|sign\left(im(X_{ab})\right)\right\}\right|}{E\{|im(X_{ab})|\}}$$

where $im\ (X_{ab})$ is the imaginary part of the cross-spectrum of the complex narrowband time series Z_a and Z_b, and $E\{\ \}$ is the expectancy value operator. The cross-spectrum X_{ab} can be substituted with $= Z_a Z_b^*$, where * denotes the complex conjugate, and the mean over samples can be taken as the expectancy value (Siebenhühner et al., 2020). The wPLI is insensitive to artificial connections arising as direct effects of zero-phase lagged linear signal mixing that is a major issue in connectivity analysis using MEG/EEG data (Palva & Palva, 2012). Spurious interactions, however,

remain as 2nd order effects even when using zero-phase lag insensitive connectivity metrics. Since spurious connections are more likely to be reported for regions with low source-reconstruction accuracy, we removed from the analysis parcels with *fidelity* < 0.2, which led to the exclusion of 9.27%, of possible parcel pairs (Korhonen et al., 2014; Siebenhühner et al., 2020).

Graph theory (Bullmore & Sporns, 2009) was used to characterize the network structures in group-level adjacency matrices. Each thresholded adjacency matrix defined a graph made up of nodes and edges, where nodes are cortical parcels and edges are the significant interactions between nodes. The mean connection strengths were obtained by averaging the strength of all valid edges in the connectome for each subject and then over subjects in each *COMT* and *BDNF* polymorphism group. For functional subsystem analysis, all pairwise interactions were averaged across the frequency bands defined by clustering analyses (Fig S1) and then collapsed into the 7 functional systems of the Yeo parcellation (Yeo et al., 2011).

Computational modelling

We used a nested Kuramoto model (Siebenhühner et al., 2020) to investigate the covariance and mutual correlations of local synchronization (node/parcel amplitude), inter-areal synchronization, and local LRTCs in a heuristic model of synchronization dynamics. The model was adapted from a conventional Kuramoto model so that it comprised 100 nodes (corresponding to 100 cortical parcels) and each node was modelled by a Kuramoto model of 500 oscillators. The model was defined so that for each node *k*, the temporal evolution of the phase θ of each oscillator *i* was described by:

$$\frac{d\theta_i^k}{dt} = \omega_i + \frac{K}{N_{osc.}} \sum_{j=1}^{N_{osc.}} sin(\theta_j - \theta_i) + \sum_{l=1}^{N_{nodes}} W_{k,l} * sin(\varphi_l - \theta_i) + N(0, \sigma)$$

where ω_i is the oscillation frequency of an oscillator, K is the local coupling (control) parameter, φ_l is the average phase of the node l, $W_{k,j}$ is the connection strength between the node k and other nodes j, and $N(0,\sigma)$ is Gaussian noise. For the connection strengths W, we used the log-scaled structural connectome of fiber counts based on the Schaefer parcellation with 100 parcels (Schaefer et al., 2018) multiplied by a global coupling (control) parameter L at L = 0.5.

Node time series mimicking the parcel time series in MEG data were obtained by averaging the complex time series of the oscillators in the node. Local synchronization was measured by the absolute value of the complex node time series (Kuramoto order) that is comparable to the amplitude of MEG parcel time series. Because modelled data, unlike MEG data, is not influenced by volume conduction (VC) we chose to estimate pairwise synchrony here with the Phase Locking Value (PLV) which in the absence of VC is roughly equivalent to wPLI, but more computationally efficient. As with MEG, we used DFA to estimate LRTC exponents. We estimated the correlation between amplitudes and DFA exponents, and between synchronization and DFA exponents, across all nodes, with Spearman's correlation coefficient.

Statistical analysis

Before statistical testing, time-series were collapsed into the 148 parcels of the original Destrieux atlas (Destrieux et al., 2011) to limit the number of comparisons and to improve statistical stability by averaging out anatomical variability, which is large across individuals. Group-level upper and lower confidence limits (2.5% and 97.5%) were computed for each polymorphism group with a bootstrapping approach, using N = 1000 resamplings with replacement of the subjects in the group.

To obtain canonical frequency bands, we first estimated spatial similarity across frequency-bands separately for oscillation amplitudes and DFA exponents using machine learning by Louvain community detection (Blondel et al., 2008) with gamma value of 1.09. This analysis identified

canonical frequency bands of theta (θ, 3–7 Hz), alpha (α, 8–14 Hz), beta (β, 14–30 Hz), and gamma (γ, 30–60 Hz) (Fig S1). We used repeated-measures analysis of variance (ANOVA) (IBM SPSS Statistics) for testing differences in the oscillation amplitudes (A) and DFA exponents averaged across all parcels between the frequency-bands. The effects of *COMT* and *BDNF* polymorphisms on oscillation amplitudes and DFAs over the whole brain were tested separately for each Morlet frequency (Fig 2A, 3A) as well as canonical frequency band (θ, α, β and γ) using univariate ANOVA with the polymorphisms as between-participants factors and age as a covariate. Partial eta squared (η_p^2) is reported as a measure of effect size.

Finally, we used the Mann-Whitney-U test ($p < 0.05$) to test pair-wise differences between the polymorphism groups separately for each wavelet frequency (Fig 2B, 3B) and parcel (Fig 2C, 3C). Multiple comparisons were initially accounted for with false discovery rate reduction (FDR) by discarding as many least-significant observations as were predicted to be false by the alpha-level (5% at $\alpha = 0.05$) for each time-frequency bin. We further estimated a threshold (see dark grey area in Figs. 2B and 3B) for the residual fraction of significants so that the probability, p_q, for finding a fraction of significant value above this threshold by chance in any single frequency out of all wavelet frequencies is $p_q < 0.05$.

For inter-areal synchronization, confidence intervals were computed with a bootstrapping approach ($N = 1000$). As the synchronization data violated the normality assumption, we tested, for each Morlet frequency, whether there was a significant difference between polymorphism groups with a nonparametric Kruskal-Wallis test ($p < 0.05$) and then used the Benjamini-Hochberg method to correct for multiple comparisons (Fig 4A). Connection density (K) of the mean connection strengths was used to index the proportion of significant edges from all possible interactions. Differences between the polymorphism groups in connectivity within and between subsystems

(Yeo et al., 2011) were then tested for statistical significance with the Kruskal-Wallis test ($p < 0.05$) and corrected for multiple comparisons with Benjamini-Hochberg (Fig 4B).

Finally, we estimated the correlation coefficient between amplitudes and DFA exponents and between synchronization and DFA exponents, for each parcel and wavelet frequency, across subjects within the polymorphism groups, using Spearman's rank correlation test. Values were then averaged across all parcels and within frequency bands. Confidence limits from 2.5% to 97.5% were obtained from bootstrapping ($N = 1000$) as above. Significance testing for difference between polymorphism groups was done with permutation statistics ($N = 1000$) where the subjects were randomly assigned, without replacement, to original-sized polymorphism groups.

Competing interests

Authors declare that they have no competing interests.

Data availability

Ethical restrictions apply to data and original data cannot be shared on a public server. Data underlying figures, statistics, and main conclusions will be uploaded to Dryad server (https://doi.org/10.5061/dryad.3n5tb2rjp) upon acceptance. All original code has been deposited at https://github.com/palvalab/RS-Gen and is publicly available as of the date of publication.

References

Arnulfo, G., Wang, S. H., Toselli, B., Myrov, V., Hirvonen, J., Fato, M., Nobili, L., Cardinale, F., Rubino, A., Zhigalov, A., Palva, S., & Palva, J. M. (2020). Long-range phase synchronization of high-frequency oscillations in human cortex. *Nature Communications, 11*, 5363. https://doi.org/10.1038/s41467-020-18975-8

Batista-Brito, R., Zagha, E., Ratliff, J. M., & Vinck, M. (2018). Modulation of cortical circuits by top-down processing and arousal state in health and disease. *Current Opinion in Neurobiology, 52*, 172-181. https://doi.org/10.1016/j.conb.2018.06.008

Beggs, J. M. (2008). The criticality hypothesis: How local cortical networks might optimize information processing. *Philosophical Transactions of The Royal Society A: Mathematics, Physical and Engineering Sciences, 366*, 329-343. https://doi.org/10.1098/rsta.2007.2092

Beste, C., Kolev, V., Yordanova, J., Domschke, K., Falkenstein, M., Baune, B. T., & Konrad, C. (2010). The role of the BDNF Val66Met polymorphism for the synchronization of error-specific neural networks. *Journal of Neuroscience, 30*(32), 10727-10733. https://doi.org/10.1523/JNEUROSCI.2493-10.2010

Betti, V., Corbetta, M., de Pasquale, F., Wens, V., & Della Penna, S. (2018). Topology of functional connectivity and hub dynamics in the beta band as temporal prior for natural vision in the human brain. *Journal of Neuroscience, 38*(15), 3858-3871. https://doi.org/10.1523/JNEUROSCI.1089-17.2018

Björklund, A., & Dunnett, S. B. (2007). Dopamine neuron systems in the brain: an update. *Trends in Neurosciences, 30*(5), 194-202. https://doi.org/10.1016/j.tins.2007.03.006

Blondel, V. D., Guillaume, J.-L., Lambiotte, R., & Lefebvre, E. (2008). Fast unfolding of communities in large networks. *Journal of statistical mechanics: theory and experiment, 10*, P10008. https://doi.org/10.1088/1742-5468/2008/10/P10008

Bodenmann, S., Rusterholz, T., Dürr, R., Stoll, C., Bachmann, V., Geissler, E., Jaggi-Schwarz, K., & Landolt, H.-P. (2009). The functional Val158Met polymorphism of COMT predicts interindividual differences in brain oscillations in young men. *Journal of Neuroscience, 29*(35), 10855-10862. https://doi.org/10.1523/JNEUROSCI.1427-09.2009

Bonetti, L., Bruzzone, S. E. P., Sedghi, N. A., Haumann, N. T., Paunio, T., Kantojärvi, K., Kliuchko, M., Vuust, P., & Brattico, E. (2021). Brain predictive coding processes are associated to COMT gene Val158Met polymorphism. *NeuroImage, 233*, 117954. https://doi.org/10.1016/j.neuroimage.2021.117954

Braun, U., Harneit, A., Pergola, G., Menara, T., Schäfer, A., Betzel, R. F., Zang, Z., Schweiger, J. I., Zhang, X., Schwarz, K., Chen, J., Blasi, G., Bertolino, A., Durstewitz, D., Pasqualetti, F., Schwarz, E., Meyer-Lindenberg, A., Bassett, D. S., & Tost, H. (2021). Brain network dynamics during working memory are modulated by dopamine and diminished in

schizophrenia. *Nature Communications*, *12*, 3478. https://doi.org/10.1038/s41467-021-23694-9

Brookes, M. J., Woolrich, M., Luckhoo, H., Price, D., Hale, J. R., Stephenson, M. C., Barnes, G. R., Smith, S. M., & Morris, P. G. (2011). Investigating the electrophysiological basis of resting state networks using magnetoencephalography. *Proceedings of the National Academy of Sciences*, *108*(40), 16783–16788. https://doi.org/www.pnas.org/cgi/doi/10.1073/pnas.1112685108

Bullmore, E., & Sporns, O. (2009). Complex brain networks: graph theoretical analysis of structural and functional systems. *Nature Reviews Neuroscience*, *10*(3), 186-198. https://doi.org/10.1038/nrn2575

Cabral, J., Kringelbach, M. L., & Deco, G. (2014). Exploring the network dynamics underlying brain activity during rest. *Progress in Neurobiology*, *114*, 102-131. https://doi.org/10.1016/j.pneurobio.2013.12.005

Castrén, E., & Monteggia, L. M. (2021). Brain-derived neurotrophic factor signaling in depression and antidepressant action. *Biological Psychiatry*, *90*, 128–136. https://doi.org/10.1016/j.biopsych.2021.05.008

Chang, C. C., Chow, C. C., Tellier, L. C., Vattikuti, S., Purcell, S. M., & Lee, J. J. (2015). Second-generation PLINK: rising to the challenge of larger and richer datasets. *Gigascience*, *4*(1), 7. https://doi.org/10.1186/s13742-015-0047-8

Chen, J., Lipska, B. K., Halim, N., Ma, Q. D., Matsumoto, M., Melhem, S., Kolachana, B. S., Hyde, T. M., Herman, M. M., Apud, J., Egan, M. F., Kleinman, J. E., & Weinberger, D. R. (2004). Functional analysis of genetic variation in catechol-O-methyltransferase (COMT): Effects on mRNA, protein, and enzyme activity in postmortem human brain. *American Journal of Human Genetics*, *75*, 807-821.

Chen, W., Chen, C., Xia, M., Wu, K., Chen, C., He, Q., Xue, G., Wang, W., He, Y., & Dong, Q. (2016). Interaction effects of BDNF and COMT genes on resting-state brain activity and working memory. *Frontiers in Human Neuroscience*, *10*, 540. https://doi.org/10.3389/fnhum.2016.00540

Chialvo, D. R. (2010). Emergent complex neural dynamics. *Nature Physics*, *6*, 744-750. https://doi.org/10.1038/NPHYS1803

Cocchi, L., Gollo, L. L., Zalesky, A., & Breakspear, M. (2017). Criticality in the brain: A synthesis of neurobiology, models and cognition. *Progress in Neurobiology*, *158*, 132-152. https://doi.org/http://dx.doi.org/10.1016/j.pneurobio.2017.07.002

Cools, R. (2019). Chemistry of the adaptive mind: Lessons from dopamine. *Neuron*, *104*(1), 113-131. https://doi.org/10.1016/j.neuron.2019.09.035

Cools, R., & D'Esposito, M. (2011). Inverted-U–shaped dopamine actions on human working memory and cognitive control. *Biological Psychiatry, 69*, e113-e125. https://doi.org/10.1016/j.biopsych.2011.03.028

Daffertshofer, A., Ton, R., Kringelbach, M. L., Woolrich, M., & Deco, G. (2018). Distinct criticality of phase and amplitude dynamics in the resting brain. *NeuroImage, 180*, 442-447. https://doi.org/10.1016/j.neuroimage.2018.03.002

Dale, A. M., Liu, A. K., Fischl, B. R., Buckner, R. L., Belliveau, J. W., Lewine, J. D., & Halgren, E. (2000). Dynamic statistical parametric mapping: combining fMRI and MEG for high-resolution imaging of cortical activity. *Neuron, 26*(1), 55-67.

Deco, G., & Jirsa, V. K. (2012). Ongoing cortical activity at rest: Criticality, multistability, and ghost attractors. *The Journal of Neuroscience, 32*(10), 3366-3375. https://doi.org/10.1523/JNEUROSCI.2523-11.2012

Deco, G., Kringelbach, M. L., Arnatkeviciute, A., Oldham, S., Sabaroedin, K., Rogasch, N. C., Aquino, K. M., & Fornito, A. (2021). Dynamical consequences of regional heterogeneity in the brain's transcriptional landscape. *Science Advances, 7*(29), eabf4752. https://doi.org/10.1126/sciadv.abf4752

Destrieux, C., Fischl, B., Dale, A., & Halgren, E. (2011). Automatic parcellation of human cortical gyri and sulci using standard anatomical nomenclature. *NeuroImage, 53*(1), 1-15. https://doi.org/10.1016/j.neuroimage.2010.06.010.

Donhauser, P. W., & Baillet, S. (2020). Two distinct neural timescales for predictive speech processing. *Neuron, 105*, 385–393. https://doi.org/10.1016/j.neuron.2019.10.019

Dosenbach, N. U. F., Fair, D. A., Cohen, A. L., Schlaggar, B. L., & Petersen, S. E. (2008). A dual-networks architecture of top-down control. *Trends in Cognitive Sciences, 12*(3), 99-105.

Egan, M. F., Kojima, M., Callicott, J. H., Goldberg, T. E., Kolachana, B. S., Bertolino, A., Zaitsev, E., Gold, B., Goldman, D., Dean, M., Lu, B., & Weinberger, D. R. (2003). The BDNF val66met polymorphism affects activity-dependent secretion of BDNF and human memory and hippocampal function. *Cell, 112*(2), 257-269.

Farrell, S. M., Tunbridge, E. M., Braeutigam, S., & Harrison, P. J. (2012). COMT Val158Met genotype determines the direction of cognitive effects produced by catechol-O-methyltransferase inhibition. *Biological Psychiatry, 71*, 538-544. https://doi.org/10.1016/j.biopsych.2011.12.023

Fell, J., & Axmacher, N. (2011). The role of phase synchronization in memory processes. *Nature Reviews Neuroscience, 12*(2), 105-118. https://doi.org/10.1038/nrn2979

Ferguson, K. A., & Cardin, J. A. (2020). Mechanisms underlying gain modulation in the cortex. *Nature Reviews Neuroscience, 21*, 80-92. https://doi.org/10.1038/ s41583-019-0253-y

Fisher, P. M., Ozenne, B., Svarer, C., Adamsen, D., Lehel, S., Baaré, W. F. C., Jensen, P. S., & Knudsen, G. M. (2017). BDNF val66met association with serotonin transporter binding in healthy humans. *Translational Psychiatry, 7*, e1029. https://doi.org/10.1038/tp.2016.295

Foster, B. L., He, B. J., Honey, C. J., Jerbi, K., Maier, A., & Saalmann, Y. B. (2016). Spontaneous neural dynamics and multi-scale network organization. *Frontiers in Systems Neuroscience, 10*(7). https://doi.org/10.3389/fnsys.2016.00007

Fries, P. (2015). Rhythms for cognition: Communication through coherence. *Neuron, 88*, 220-235. https://doi.org/http://dx.doi.org/10.1016/j.neuron.2015.09.034

Garcia-Garcia, M., Via, M., Zarnowiec, K., SanMiguel, I., Escera, C., & Clemente, I. C. (2017). COMT and DRD2/ANKK-1 gene-gene interaction account for resetting of gamma neural oscillations to auditory stimulus-driven attention. *PLoS ONE, 12*(2), e0172362. https://doi.org/10.1371/journal.pone.0172362

Gener, T., Tauste Campo, A., Alemany-González, M., Nebot, P., Delgado-Sallent, C., Chanovas, J., & Puig, M. V. (2019). Serotonin 5-HT1A, 5-HT2A and dopamine D2 receptors strongly influence prefronto-hippocampal neural networks in alert mice: Contribution to the actions of risperidone. *Neuropharmacology, 158*, 107743. https://doi.org/10.1016/j.neuropharm.2019.107743

Gramfort, A., Luessi, M., Larson, E., Engemann, D. A., Strohmeier, D., Brodbeck, C., Parkkonen, L., & Hämäläinen, M. S. (2014). MNE software for processing MEG and EEG data. *NeuroImage, 86*, 446-460. https://doi.org/http://dx.doi.org/10.1016/j.neuroimage.2013.10.027

Grasby, K. L., Jahanshad, N., & al., e. (2020). The genetic architecture of the human cerebral cortex. *Science, 367*(6484), eaay6690. https://doi.org/10.1126/science.aay6690

Hahn, A., Breakspear, M., Rischka, L., Wadsak, W., Godbersen, G. M., Pichler, V., Michenthaler, P., Vanicek, T., Hacker, M., Kasper, S., Lanzenberger, R., & Cocchi, L. (2020). Reconfiguration of functional brain networks and metabolic cost converge during task performance. *ELife, 9*, e52443. https://doi.org/10.7554/eLife.52443

Hardstone, R., Poil, S.-S., Schiavone, G., Jansen, R., Nikulin, V. V., Mansvelder, H. D., & Linkenkaer-Hansen, K. (2012). Detrended fluctuation analysis: a scale-free view on neuronal oscillations. *Frontiers in Physiology, 3*(Article 450), 1-13. https://doi.org/10.3389/fphys.2012.00450

Hariri, A. R., Goldberg, T. E., Mattay, V. S., Kolachana, B. S., Callicott, J. H., Egan, M. F., & Weinberger, D. R. (2003). Brain-derived neurotrophic factor val66met polymorphism affects human memory-related hippocampal activity and predicts memory performance. *Journal of Neuroscience, 23*(17), 6690-6694.

Harris, K. D., & Thiele, A. (2011). Cortical state and attention. *Nature Reviews Neuroscience, 12*(9), 509-523. https://doi.org/10.1038/nrn3084

Hiltunen, T., Kantola, J., Elseoud, A. A., Lepola, P., Suominen, K., Starck, T., Nikkinen, J., Remes, J., Tervonen, O., Palva, S., Kiviniemi, V., & Palva, J. M. (2014). Infra-slow EEG fluctuations are correlated with resting-state network dynamics in fMRI. *Journal of Neuroscience, 34*(2), 356 –362. https://doi.org/10.1523/JNEUROSCI.0276-13.2014

Hipp, J. F., & Siegel, M. (2015). BOLD fMRI correlation reflects frequency-specific neuronal correlation. *Current Biology, 25*, 1368-1374. https://doi.org/http://dx.doi.org/10.1016/j.cub.2015.03.049

Jensen, O., Gips, B., Bergmann, T. O., & Bonnefond, M. (2014). Temporal coding organized by coupled alpha and gamma oscillations prioritize visual processing. *Trends in Neurosciences, 37*(7), 357-369. https://doi.org/10.1016/j.tins.2014.04.001

Kinouchi, O., & Copelli, M. (2006). Optimal dynamical range of exitable networks at criticality. *Nature Physics, 2*, 348-351. https://doi.org/10.1038/nphys289

Klimesch, W., Sauseng, P., & Hanslmayr, S. (2007). EEG alpha oscillations: The inhibition–timing hypothesis. *Brain Research Reviews, 51*(1), 63-88. https://doi.org/10.1016/j.brainresrev.2006.06.003

Korhonen, O., Palva, S., & Palva, J. M. (2014). Sparse weightings for collapsing inverse solutions to cortical parcellations optimize M/EEG source reconstruction accuracy. *Journal of Neuroscience Methods, 226*, 147-160. https://doi.org/http://dx.doi.org/10.1016/j.jneumeth.2014.01.031

Lee, S.-H., & Dan, Y. (2012). Neuromodulation of brain states. *Neuron, 76*(1), 109-222. https://doi.org/10.1016/j.neuron.2012.09.012

Leppäaho, E., Renvall, H., Salmela, E., Kere, J., Salmelin, R., & Kaski, S. (2019). Discovering heritable modes of MEG spectral power. *Human Brain Mapping, 40*(5), 1391-1402. https://doi.org/10.1002/hbm.24454

Linkenkaer-Hansen, K., Nikouline, V. V., Palva, J. M., & Ilmoniemi, R. J. (2001). Long-range temporal correlations and scaling behavior in human brain oscillations. *Journal of Neuroscience, 21*(4), 1370–1377.

Linkenkaer-Hansen, K., Smit, D. J. A., Barkil, A., van Beijsterveldt, T. E. M., Brussaard, A. B., Boomsma, D. I., van Ooyen, A., & de Geus, E. J. C. (2007). Genetic contributions to long-range temporal correlations in ongoing oscillations. *Journal of Neuroscience, 27*(50), 13882–13889. https://doi.org/10.1523/JNEUROSCI.3083-07.2007

Lucki, I. (1988). The spectrum of behaviors influenced by serotonin. *Biological psychiatry, 44*, 151–162.

Mahjoory, K., Schoffelen, J.-M., Keitel, A., & Gross, J. (2020). The frequency gradient of human resting- state brain oscillations follows cortical hierarchies. *ELife, 9*, e53715. https://doi.org/10.7554/eLife.53715

Manninen, S., Karjalainen, T., Tuominen, L. J., Hietala, J., Kaasinen, V., Joutsa, J., Rinne, J., & Nummenmaa, L. (2021). Cerebral grey matter density is associated with neuroreceptor and neurotransporter availability: A combined PET and MRI study. *NeuroImage, 235*, 117968. https://doi.org/10.1016/j.neuroimage.2021.117968

Männistö, P. T., & Kaakkola, S. (1999). Catechol-O-methyltransferase (COMT): biochemistry, molecular biology, pharmacology, and clinical efficacy of the new selective COMT inhibitors. *Pharmacological reviews, 51*(4), 593-628.

Marzetti, L., Basti, A., Chella, F., D'Andrea, A., Syrjälä, J., & Pizzella, V. (2019). Brain functional connectivity through phase coupling of neuronal oscillations: A perspective from magnetoencephalography. *Frontiers in Neuroscience, 13*, 964. https://doi.org/10.3389/fnins.2019.00964

Marzetti, L., Della Penna, S., Snyder, A. Z., Pizzella, V., Nolte, G., de Pasquale, F., Romani, G. L., & Corbetta, M. (2013). Frequency specific interactions of MEG resting state activity within and across brain networks as revealed by the multivariate interaction measure. *NeuroImage, 79*, 172-183. https://doi.org/http://dx.doi.org/10.1016/j.neuroimage.2013.04.062

Matsuo, K., Walss-Bass, C., Nery, F. G., Nicoletti, M. A., Hatch, J. P., Frey, B. N., Monkul, E. S., Zunta-Soares, G. B., Bowden, C. L., Escamilla, M. A., & Soares, J. C. (2009). Neuronal correlates of brain-derived neurotrophic factor Val66Met polymorphism and morphometric abnormalities in bipolar disorder. *Neuropsychopharmacology, 34*, 1904-1913. https://doi.org/10.1038/npp.2009.23

McLoughlin, G., Palmer, J. A., Rijsdijk, F., & Makeig, S. (2014). Genetic overlap between evoked frontocentral theta-band phase variability, reaction time variability, and Attention-Deficit/Hyperactivity Disorder symptoms in a twin study. *Biological Psychiatry, 75*, 238-247. https://doi.org/10.1016/j.biopsych.2013.07.020

Meyer-Lindenberg, A., Kohn, P. D., Kolachana, B. S., Kippenhan, S., McInerney-Leo, A., Nussbaum, R., Weinberger, D. R., & Berman, K. F. (2005). Midbrain dopamine and prefrontal function in humans: interaction and modulation by COMT genotype. *Nature Neuroscience, 8*, 594-596. https://doi.org/10.1038/nn1438

Mier, D., Kirsch, P., & Meyer-Lindenberg, A. (2010). Neural substrates of pleiotropic action of genetic variation in COMT: a meta-analysis. *Molecular Psychiatry, 15*, 918-927. https://doi.org/10.1038/mp.2009.36

Monto, S., Palva, S., Voipio, J., & Palva, J. M. (2008). Very slow EEG fluctuations predict the dynamics of stimulus detection and oscillation amplitudes in humans. *Journal of Neuroscience, 28*(33), 8268 – 8272. https://doi.org/10.1523/JNEUROSCI.1910-08.2008

Mostame, P., & Sadaghiani, S. (2020). Oscillation-based connectivity architecture is dominated by an intrinsic spatial organization, not cognitive state or frequency. *Journal of Neuroscience*. https://doi.org/10.1523/JNEUROSCI.2155-20.2020

Munn, B. R., Müller, E. J., Wainstein, G., & Shine, J. M. (2021). The ascending arousal system shapes neural dynamics to mediate awareness of cognitive states. *Nature Communications, 12*, 6016 https://doi.org/10.1038/s41467-021-26268-x

Newbold, D. J., Gordon, E. M., Laumann, T. O., Seider, N. A., Montez, D. F., Gross, S. J., Zheng, A., Nielsen, A. N., Hoyt, C. R., Hampton, J. M., Ortega, M., Adeyemo, B., Miller, D. B., Van, A. N., Marek, S., Schlaggar, B. L., Carter, A. R., Kay, B. P., Greene, D. J., Raichle, M. E., Petersen, S. E., Snyder, A. Z., & Dosenbach, N. U. F. (2021). Cingulo-opercular control network and disused motor circuits joined in standby mode. *Proceedings of the National Academy of Sciences, 118*(13), e2019128118. https://doi.org/10.1073/pnas.2019128118

Notaras, M., Hill, R., & van den Buuse, M. (2015). The BDNF gene Val66Met polymorphism as a modifier of psychiatric disorder susceptibility: progress and controversy. *Molecular Psychiatry, 20*, 916–930. https://doi.org/10.1038/mp.2015.27

Oostenveld, R., Fries, P., Maris, E., & Schoffelen, J.-M. (2011). FieldTrip: Open Source Software for Advanced Analysis of MEG, EEG, and Invasive Electrophysiological Data. *Computational intelligence and neuroscience, 1*. https://doi.org/10.1155/2011/156869

Oswald, V., Zerouali, Y., Boulet-Craig, A., Krajinovic, M., Laverdière, C., Sinnett, D., Jolicoeur, P., Lippé, S., Jerbi, K., & Robaey, P. (2017). Spontaneous brain oscillations as neural fingerprints of working memory capacities: A resting-state MEG study. *Cortex, 97*, 109-124. https://doi.org/10.1016/j.cortex.2017.09.021

Ott, T., & Nieder, A. (2019). Dopamine and cognitive control in prefrontal cortex. *Trends in Cognitive Sciences, 23*(3), 213-234. https://doi.org/10.1016/j.tics.2018.12.006

Palva, J. M., Monto, S., Kulashekhar, S., & Palva, S. (2010). Neuronal synchrony reveals working memory networks and predicts individual memory capacity. *Proceedings of the National Academy of Sciences, 107*(16), 7580-7585. https://doi.org/www.pnas.org/cgi/doi/10.1073/pnas.0913113107

Palva, J. M., Wang, S. H., Palva, S., Zhigalov, A., Monto, S., Brookes, M. J., Schoffelen, J.-M., & Jerbi, K. (2018). Ghost interactions in MEG/EEG source space: A note of caution on inter-areal coupling measures. *NeuroImage, 173*, 632–643. https://doi.org/10.1016/j.neuroimage.2018.02.032

Palva, J. M., Zhigalov, A., Hirvonen, J., Korhonen, O., Linkenkaer-Hansen, K., & Palva, S. (2013). Neuronal long-range temporal correlations and avalanche dynamics are correlated with behavioral scaling laws. *Proceedings of the National Academy of Sciences, of the USA, 110*(9), 3585–3590. https://doi.org/www.pnas.org/cgi/doi/10.1073/pnas.1216855110

Palva, S., & Palva, J. M. (2012). Discovering oscillatory interaction networks with M/EEG: challenges and breakthroughs. *Trends in Cognitive Sciences, 16*(4), 219-230. https://doi.org/10.1016/j.tics.2012.02.004

Palva, S., & Palva, J. M. (2018). Roles of brain criticality and multiscale oscillations in temporal predictions for sensorimotor processing. *Trends in Neurosciences, 41*(10), 729-743. https://doi.org/https://doi.org/10.1016/j.tins.2018.08.008

Papenberg, G., Karalija, N., Salami, A., Rieckmann, A., Andersson, M., Axelsson, J., Riklund, K., Lindenberger, U., Lövdén, M., Nyberg, L., & Bäckman, L. (2020). Balance between transmitter availability and dopamine D2 receptors in prefrontal cortex influences memory functioning. *Cerebral Cortex, 30*, 989-1000. https://doi.org/10.1093/cercor/bhz142

Park, H., & Poo, M. m. (2013). Neurotrophin regulation of neural circuit development and function. *Nature Reviews Neuroscience, 14*(1), 7-23. https://doi.org/10.1038/nrn3379

Parkin, G. M., Udawela, M., Gibbons, A., Scarr, E., & Dean, B. (2018). Catechol-O-methyltransferase (COMT) genotypes are associated with varying soluble, but not membrane-bound COMT protein in the human prefrontal cortex. *Journal of human genetics, 63*(12), 1251-1258. https://doi.org/10.1038/s10038-018-0511-2

Pereira, L. P., Köhler, C. A., Stubbs, B., Miskowiak, K. W., Morris, G., de Freitas, B. P., Thompson, T., Fernandes, B. S., Brunoni, A. R., Maes, M., Pizzagalli, D. A., & Carvalho, A. F. (2018). Imaging genetics paradigms in depression research: Systematic review and T meta-analysis. *Progress in Neuropsychopharmacology & Biological Psychiatry, 86*, 102-113. https://doi.org/10.1016/j.pnpbp.2018.05.012

Pfeffer, T., Ponce-Alvarez, A., Tsetsos, K., Meindertsma, T., Gahnström, C. J., van den Brink, R. L., Nolte, G., Engel, A. K., Deco, G., & Donner, T. H. (2021). Circuit mechanisms for the chemical modulation of cortex-wide network interactions and behavioral variability. *Science Advances, 7*, eabf5620. https://doi.org/10.1126/sciadv.abf5620

Plenz, D., & Thiagarajan, T. C. (2007). The organizing principles of neuronal avalanches: cell assemblies in the cortex? *Trends in Neurosciences, 30*(3), 101-110. https://doi.org/10.1016/j.tins.2007.01.005

Poil, S.-S., Hardstone, R., Mansvelder, H. D., & Linkenkaer-Hansen, K. (2012). Critical-state dynamics of avalanches and oscillations jointly emerge from balanced excitation/Inhibition in neuronal networks. *Journal of Neuroscience, 32*(29), 9817-9823. https://doi.org/10.1523/JNEUROSCI.5990-11.2012

Posthuma, D., de Geus, E. J. C., & Boomsma, D. I. (2001). Perceptual speed and IQ are associated through common genetic factors. *Behavior Genetics, 31*(6), 593-602.

Priesemann, V., Wibral, M., Valderrama, M., Pröpper, R., Le Van Quyen, M., Geisel, T., Triesch, J., Nikolic, D., & Munk, M. H. J. (2014). Spike avalanches in vivo suggest a driven, slightly subcritical brain state. *Frontiers in Systems Neuroscience, 8*, 108. https://doi.org/10.3389/fnsys.2014.00108

Puig, M. V., & Gulledge, A. T. (2011). Serotonin and prefrontal cortex function: Neurons, networks, and circuits. *Molecular Neurobiology, 44*.

Pusil, S., López, M. E., Cuesta, P., Bruña, R., Pereda, E., & Maestú, F. (2019). Hypersynchronization in mild cognitive impairment: the 'X' model. *Brain*, *142*, 3936–3950. https://doi.org/10.1093/brain/awz320

Robbins, T. W., & Arnsten, A. F. T. (2009). The neuropsychopharmacology of fronto-executive function: monoaminergic modulation. *Annual Review of Neuroscience*, *32*, 267-287. https://doi.org/10.1146/annurev.neuro.051508.135535

Salmela, E., Renvall, H., Kujala, J., Hakosalo, O., Illman, M., Vihla, M., Leinonen, E., Salmelin, R., & Kere, J. (2016). Evidence for genetic regulation of the human parieto-occipital 10-Hz rhythmic activity. *European Journal of Neuroscience*, *44*, 1963–1971. https://doi.org/10.1111/ejn.13300

Samaha, J., Iemi, L., Haegens, S., & Busch, N. A. (2020). Spontaneous brain oscillations and perceptual decision-making. *Trends in Cognitive Sciences*, *24*(8), 639-653. https://doi.org/10.1016/j.tics.2020.05.004

Schaefer, A., Kong, R., Gordon, E. M., Laumann, T. O., Zuo, X.-N., Holmes, A. J., Eickhoff, S. B., & Yeo, B. T. T. (2018). Local-Global Parcellation of the Human Cerebral Cortex from Intrinsic Functional Connectivity MRI. *Cerebral Cortex*, *28*, 3095–3114. https://doi.org/10.1093/cercor/bhx179

Schirner, M., Randal McIntosh, A., Jirsa, V., Deco, G., & Ritter, P. (2018). Inferring multi-scale neural mechanisms with brain network modelling. *ELife*, *7*, e28927. https://doi.org/10.7554/eLife.28927

Shew, W. L., & Plenz, D. (2013). The functional benefits of criticality in the cortex. *The Neuroscientist*, *19*(1), 88-100. https://doi.org/10.1177/1073858412445487

Shew, W. L., Yang, H., Petermann, T., Roy, R., & Plenz, D. (2009). Neuronal avalanches imply maximum dynamic range in cortical networks at criticality. *Journal of Neuroscience*, *29*(49), 15595–15600. https://doi.org/10.1523/JNEUROSCI.3864-09.2009

Siebenhühner, F., Wang, S. H., Arnulfo, G., Lampinen, A., Nobili, L., Palva, J. M., & Palva, S. (2020). Genuine cross-frequency coupling networks in human resting-state electrophysiological recordings. *PLoS Biology*, *18*(5), e3000685. https://doi.org/10.1371/journal.pbio.3000685

Siebenhühner, F., Wang, S. H., Palva, J. M., & Palva, S. (2016). Cross-frequency synchronization connects networks of fast and slow oscillations during visual working memory maintenance. *ELife*, *5*, e13451. https://doi.org/10.7554/eLife.13451

Siegel, M., Donner, T. H., & Engel, A. K. (2012). Spectral fingerprints of large-scale neuronal interactions. *Nature Reviews Neuroscience*, *13*, 121-134. https://doi.org/10.1038/nrn3137

Simola, J., Zhigalov, A., Morales-Muños, I., Palva, J. M., & Palva, S. (2017). Critical dynamics of endogenous fluctuations predict cognitve flexibility in the Go/NoGo task. *Scientific Reports*, *7*, 2909. https://doi.org/10.1038/s41598-017-02750-9

Singer, W. (1999). Neuronal synchrony: a versatile code for the definition of relations? *Neuron, 24*, 49-65.

Smit, D. J. A., Linkenkaer-Hansen, K., & de Geus, E. J. C. (2013). Long-range temporal correlations in resting-state alpha oscillations predict human timing-error dynamics. *Journal of Neuroscience, 33*(27), 11212-11220. https://doi.org/10.1523/JNEUROSCI.2816-12.2013

Smit, D. J. A., Wright, M. J., Meyers, J. L., Martin, N. G., Ho, Y. Y. W., Malone, S. M., Zhang, J., Burwell, S. J., Chorlian, D. B., de Geus, E. J. C., Denys, D., Hansell, N. K., Hottenga, J.-J., McGue, M., van Beijsterveldt, C. E. M., Jahanshad, N., Thompson, P. M., Whelan, C. D., Medland, S. E., Porjesz, B., Lacono, W. G., & Boomsma, D. I. (2018). Genome-wide association analysis links multiple psychiatric liability genes to oscillatory brain activity. *Human Brain Mapping, 39*, 4183-4195. https://doi.org/10.1002/hbm.24238

Stephani, T., Waterstraat, G., Haufe, S., Curio, G., Villringer, A., & Nikulin, V. V. (2020). Temporal signatures of criticality in human cortical excitability as probed by early somatosensory responses. *Jounal of Neuroscience, 40*(34), 6572-6583. https://doi.org/10.1523/JNEUROSCI.0241-20.2020

Štrac, D. S. v., Pivac, N., & Mück-Šeler, D. (2016). The serotonergic system and cognitive function. *Translational neuroscience, 7*(1), 35-49. https://doi.org/10.1515/tnsci-2016-0007

Taulu, S., Simola, J., & Kajola, M. (2005). Applications of the signal space separation method. *IEEE transactions on signal processing, 53*(9), 3359-3372. https://doi.org/10.1109/TSP.2005.853302

Thiery, T., Lajnef, T., Combrisson, E., Dehgan, A., Rainville, P., Mashour, G. A., Blain-Moraes, S., & Jerbi, K. (2018). Long-range temporal correlations in the brain distinguish conscious wakefulness from induced unconsciousness. *NeuroImage, 179*, 30–39. https://doi.org/10.1016/j.neuroimage.2018.05.069

Thut, G., Miniussi, C., & Gross, J. (2012). The functional importance of rhythmic activity in the brain. *Current Biology, 22*(16), R658-R663. https://doi.org/10.1016/j.cub.2012.06.061

Totah, N. K. B., Logothetis, N. K., & Eschenko, O. (2019). Noradrenergic ensemble-based modulation of cognition over multiple timescales. *Brain Research, 1709*, 50-66. https://doi.org/10.1016/j.brainres.2018.12.031

Tunbridge, E. M., Narajos, M., Harrison, C. H., Beresford, C., Cipriani, A., & Harrison, P. J. (2019). Which dopamine polymorphisms are functional? Systematic review and meta-analysis of COMT, DAT, DBH, DDC, DRD1–5, MAOA, MAOB, TH, VMAT1, and VMAT2. *Biological Psychiatry, 88*, 608-620. https://doi.org/10.1016/j.biopsych.2019.05.014

van den Brink, R. L., Niuwenhuis, S., & Donner, T. H. (2018). Amplification and suppression of distinct brainwide activity patterns by catecholamines. *Journal of Neuroscience, 38*(34), 7476–7491. https://doi.org/10.1523/JNEUROSCI.0514-18.2018

van den Brink, R. L., Preffer, T., & Donner, T. H. (2019). Brainstem modulation of large-scale intrinsic cortical activity correlations. *Frontiers in Human Neuroscience, 13*, 340. https://doi.org/10.3389/fnhum.2019.00340

Van Pelt, S., Boomsma, D. I., & Fries, P. (2012). Magnetoencephalography in twins reveals a strong genetic determination of the peak frequency of visually induced gamma-band synchronization. *Journal of Neuroscience, 32*(10), 3388-3392. https://doi.org/10.1523/JNEUROSCI.5592-11.2012

Vidaurre, D., Llerad, A., Smithc, S. M., & Woolrich, M. W. (2021). Behavioural relevance of spontaneous, transient brain network interactions in fMRI. *NeuroImage, 229*, 117713. https://doi.org/10.1016/j.neuroimage.2020.117713

Vijayraghavan, S., Wang, M., Birnbaum, S. G., Williams, G. V., & Arnsten, A. F. T. (2007). Inverted-U dopamine D1 receptor actions on prefrontal neurons engaged in working memory. *Nature Neuroscience, 10*(3), 376-384. https://doi.org/10.1038/nn1846

Vinck, M., Oostenveld, R., van Wingerden, M., Battaglia, F., & Pennartz, C. M. A. (2011). An improved index of phase-synchronization for electrophysiological data in the presence of volume-conduction, noise and sample-size bias. *NeuroImage, 55*(4), 1548-1565. https://doi.org/10.1016/j.neuroimage.2011.01.055

Wiencke, K., Horstmann, A., Mathar, D., Villringer, A., & Neumann, J. (2020). Dopamine release, diffusion and uptake: A computational model for synaptic and volume transmission. *PLoS Computational Biology, 16*(11), e1008410. https://doi.org/10.1371/journal.pcbi.1008410

Winkel, F., Ryazantseva, M., Voigt, M. B., Didio, G., Lilja, A., Pou, M. L., Steinzeig, A., Harkki, J., Englund, J., Khirug, S., Rivera, C., Palva, S., Taira, T., Lauri, S. E., Umemori, J., & Castrén, E. (2021). Pharmacological and optical activation of TrkB in Parvalbumin interneurons regulate intrinsic states to orchestrate cortical plasticity. *Molecular Psychiatry*. https://doi.org/10.1038/s41380-021-01211-0

Womelsdorf, T., Valiante, Taufik A , Sahin, N. T., Miller, K. J., & Tiesinga, P. (2014). Dynamic circuit motifs underlying rhythmic gain control, gating and integration. *Nature Neuroscience, 17*(8), 1031-1039. https://doi.org/10.1038/nn.3764

Yeo, B. T. T., Krienen, F. M., Sepulcre, J., Sabuncu, M. R., Lashkari, D., Hollinshead, M., Roffman, J. L., Smoller, J. W., Zöllei, L., Polimeni, J. R., Fischl, B., Liu, H., & Buckner, R. L. (2011). The organization of the human cerebral cortex estimated by intrinsic functional connectivity. *Journal of Neurophysiology, 106*, 1125-1165. https://doi.org/10.1152/jn.00338.2011.

Zagrebelsky, M., & Korte, M. (2014). Form follows function: BDNF and its involvement in sculpting the function and structure of synapses. *Neuropharmacology, 76*, 628e638. https://doi.org/10.1016/j.neuropharm.2013.05.029

Zhigalov, A., Arnulfo, G., Nobili, L., Palva, S., & Palva, J. M. (2015). Relationship of fast-and slow-timescale neuronal dynamics in human MEG and SEEG. *The Journal of Neuroscience, 35*(13), 5385-5396.

Zhigalov, A., Arnulfo, G., Nobili, L., Palva, S., & Palva, J. M. (2017). Modular co-organization of functional connectivity and scale-free dynamics in the human brain. *Network Neuroscience, 1*(2), 143-165. https://doi.org/https://doi.org/10.1162/netn_a_00008

Appendix

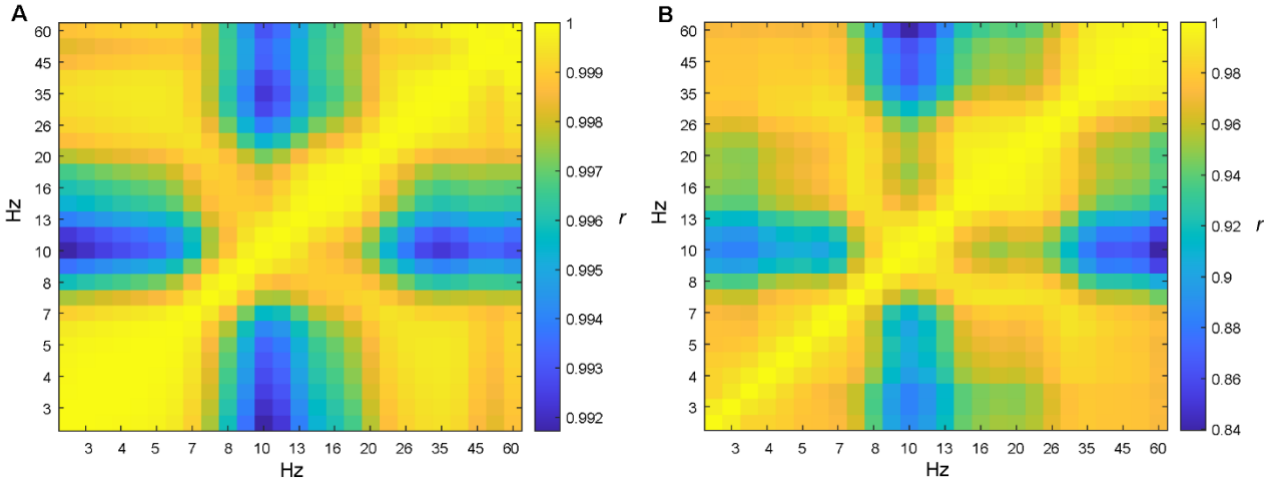

Fig S1. Frequency-band clustering. Spatial similarity across frequency-bands obtained by Louvain community detection (Blondel et al., 2008) for (A) oscillation amplitudes and (B) DFA exponents averaged across participants (N = 82). The clustering on spatial similarity yielded the frequency–frequency-band clusters of theta (θ, 3–7 Hz), alpha (α, 8–14 Hz), beta (β, 14–30 Hz), and gamma (γ, 30–60 Hz) bands. The color scales indicate the correlation coefficients.

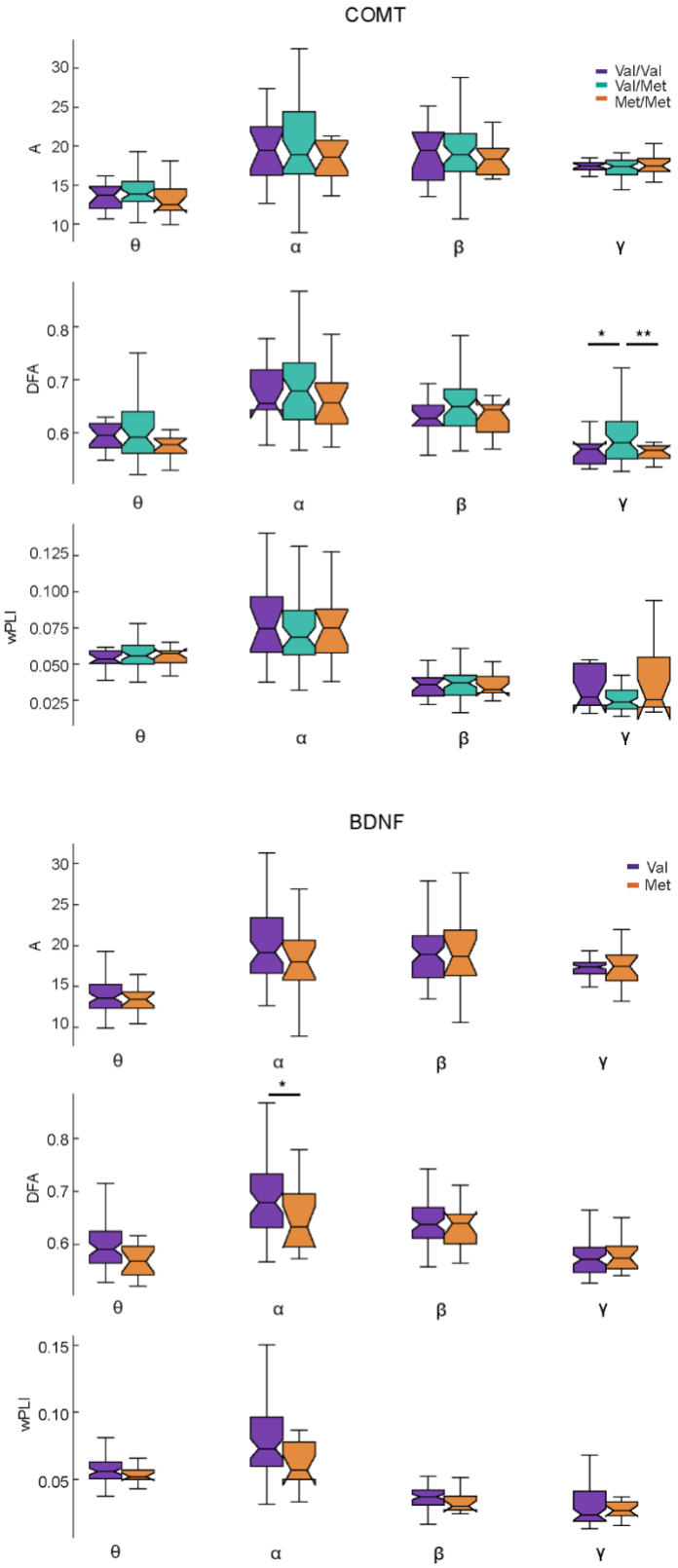

Fig S2. Whole brain averaged oscillation amplitudes, DFA and phase synchronization. Box plots of A, DFA and wPLI averaged over theta (θ, 3–7 Hz), alpha (α, 8–14 Hz), beta (β, 14–30 Hz), and gamma (γ, 30–60 Hz) frequency bands separately for each *COMT* (Val/Val in purple n = 18, Val/Met in turquoise n = 48, and Met/Met in orange n = 16) and *BDNF* polymorphism (Val/Val in

purple n = 66 and combined Val/Met & Met/Met in orange n = 16) groups. The box ends indicate the lower quartile (Q1, 25th percentile) and upper quartile (Q3, 75th percentile). The central notches denote the median, and the whiskers correspond to the range of Q1 – 1.5 * IQR and Q3 + 1.5 * IQR (where IQR is the inter-quartile range) and give roughly a 95% CI for comparing the medians. Asterisks denote significant group differences (*: $p < 0.05$, *: $p < 0.01$, t-test with unequal variances).

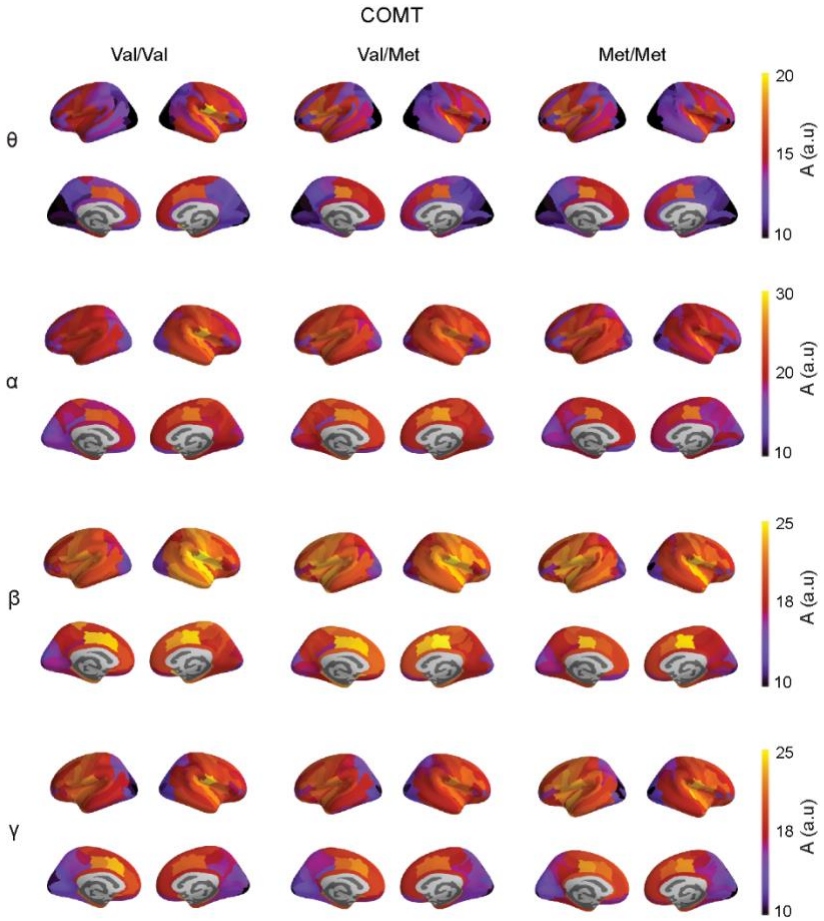

Fig S3. Mean oscillation amplitudes for *COMT* polymorphism groups. Mean amplitudes separately for each *COMT* (Val/Val, Val/Met, and Met/Met) polymorphism group averaged over theta (θ, 3–7 Hz), alpha (α, 8–14 Hz), beta (β, 14–30 Hz), and gamma (γ, 30–60 Hz) frequency bands plotted on inflated cortical surface. The color indicates the strength of the oscillations. Note that the scales vary across the frequency bands.

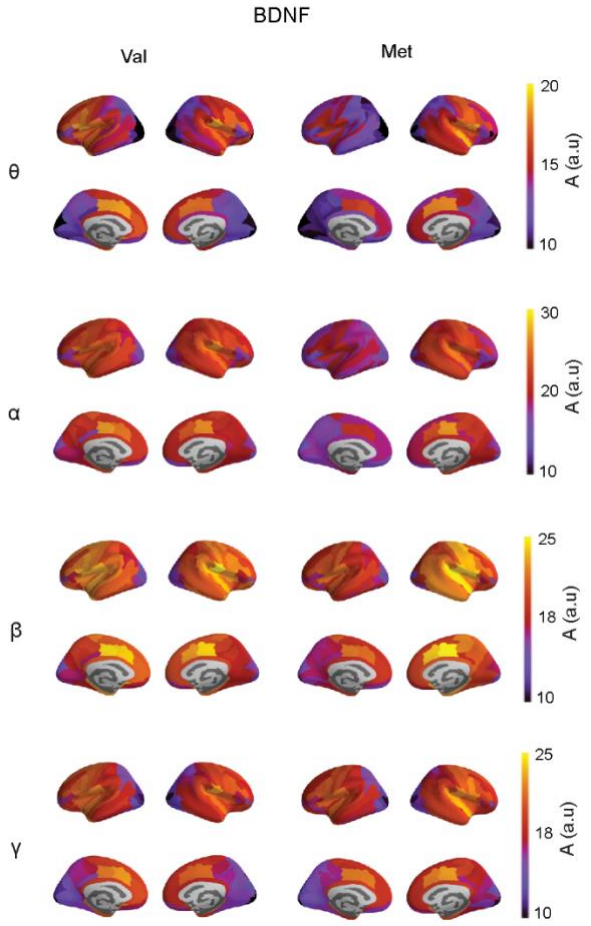

Fig S4. Mean oscillation amplitudes for *BDNF* polymorphisms. Mean amplitudes separately for each *BDNF* polymorphism (Val/Val and Met-carriers) group averaged over theta (θ, 3–7 Hz), alpha (α, 8–14 Hz), beta (β, 14–30 Hz), and gamma (γ, 30–60 Hz) frequency bands plotted on inflated cortical surface. The color indicates the strength of the oscillations. Note that the scales vary across the frequency bands.

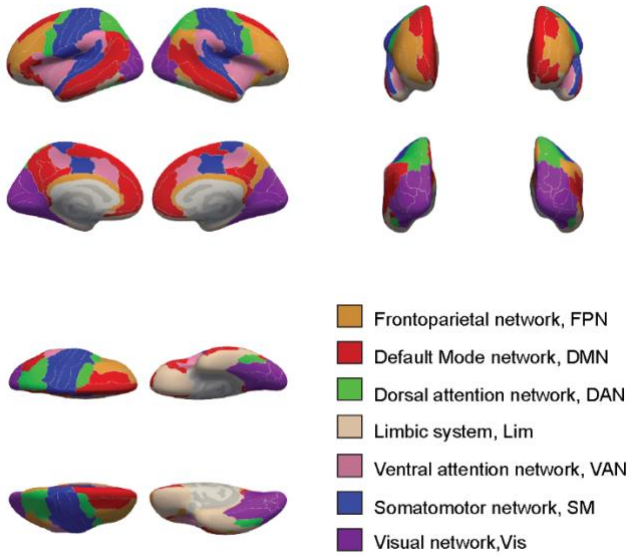

Fig S5. The functional subsystems. Cortical parcels of the Destrieux atlas (Destrieux et al., 2011) plotted on inflated cortical surface. Color indicates the functional subsystems defined by fMRI functional connectivity (Yeo et al., 2011).

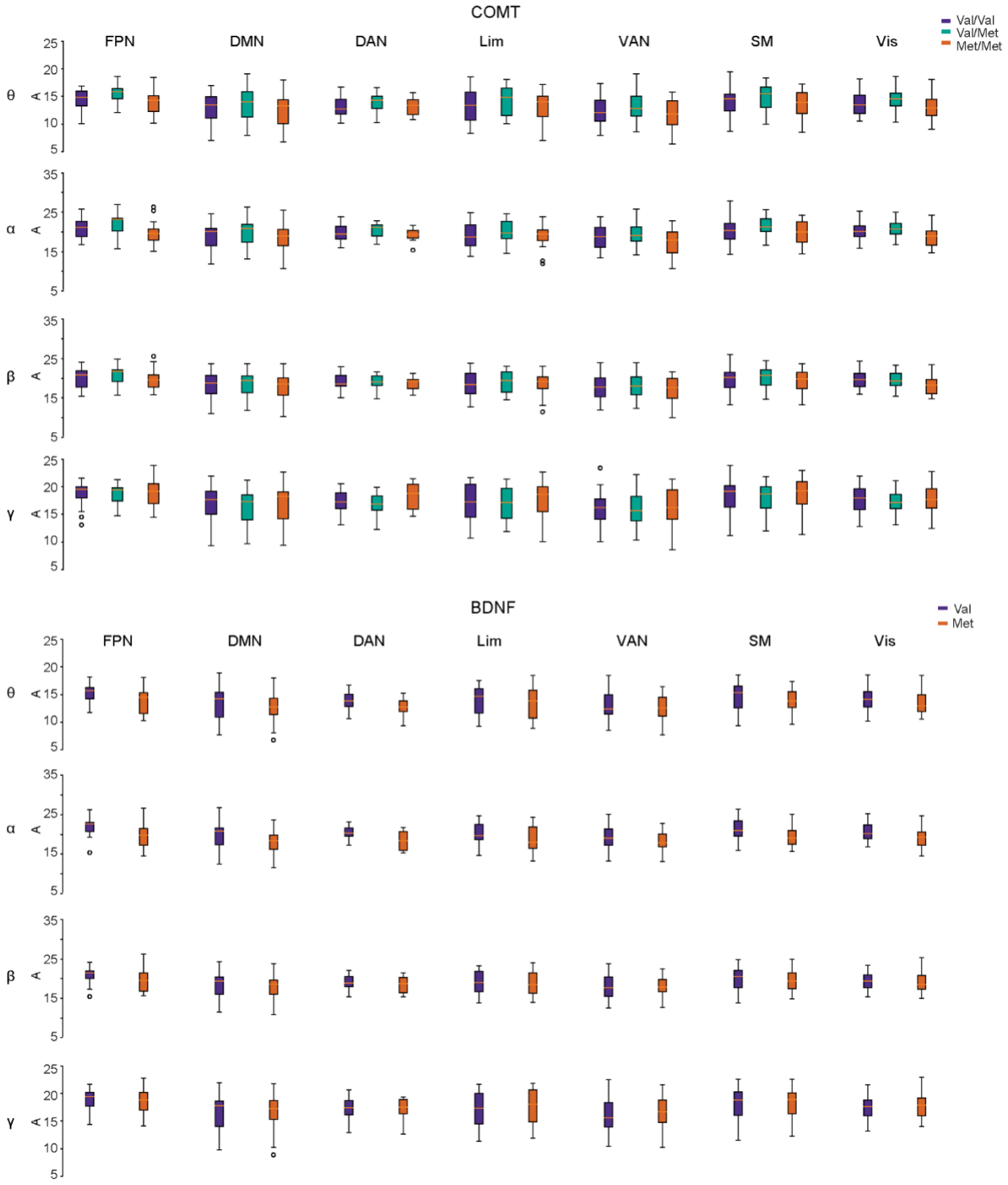

Fig S6. Mean oscillation amplitudes across the functional subsystems. Box plots of A averaged over the functional subsystems across the frequency bands: theta (θ, 3–7 Hz), alpha (α, 8–14 Hz), beta (β, 14–30 Hz), and gamma (γ, 30–60 Hz) and separately for each *COMT* (Val/Val, Val/Met, and Met/Met, upper panels) and each *BDNF* (Val/Val and Met-carriers, lower panels) polymorphism group. Abbreviations of the functional subsystems as in S5 Fig and box plot details as in S2 Fig.

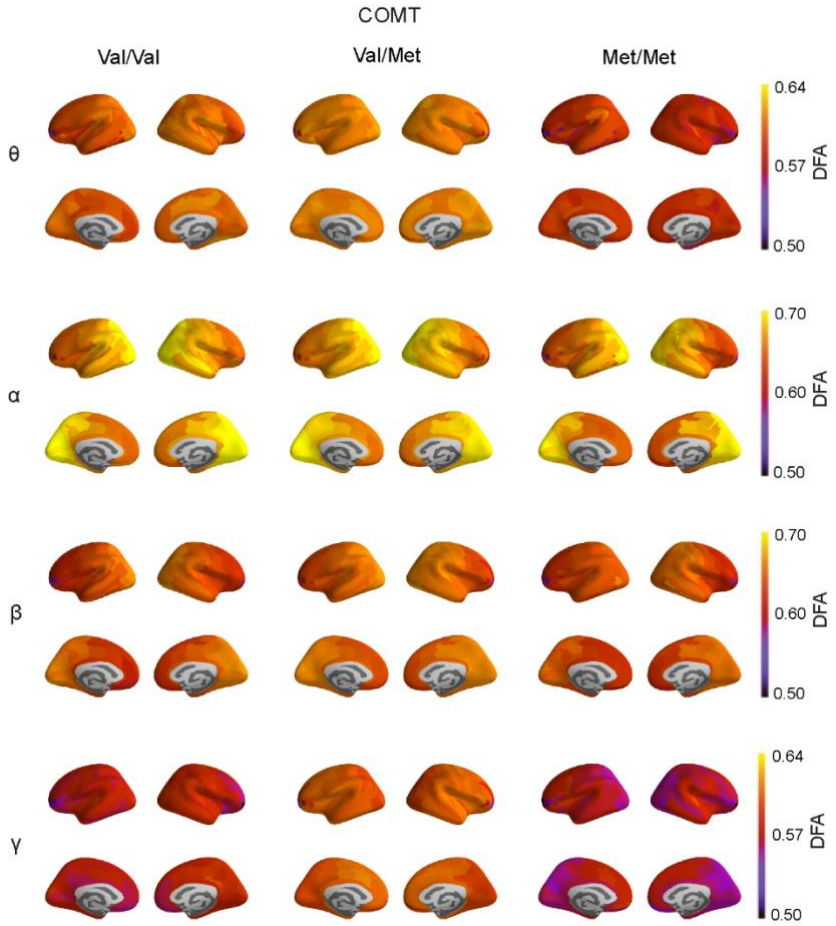

Fig S7. Mean LRTCs for *COMT* polymorphisms. Mean DFA exponents are plotted separately for each *COMT* (Val/Val, Val/Met, and Met/Met) group, averaged over theta (θ, 3–7 Hz), alpha (α, 8–14 Hz), beta (β, 14–30 Hz), and gamma (γ, 30–60 Hz) frequency bands plotted on inflated cortical surface. The color indicates the strength of the DFA exponents. Note that the scales vary across the frequency bands.

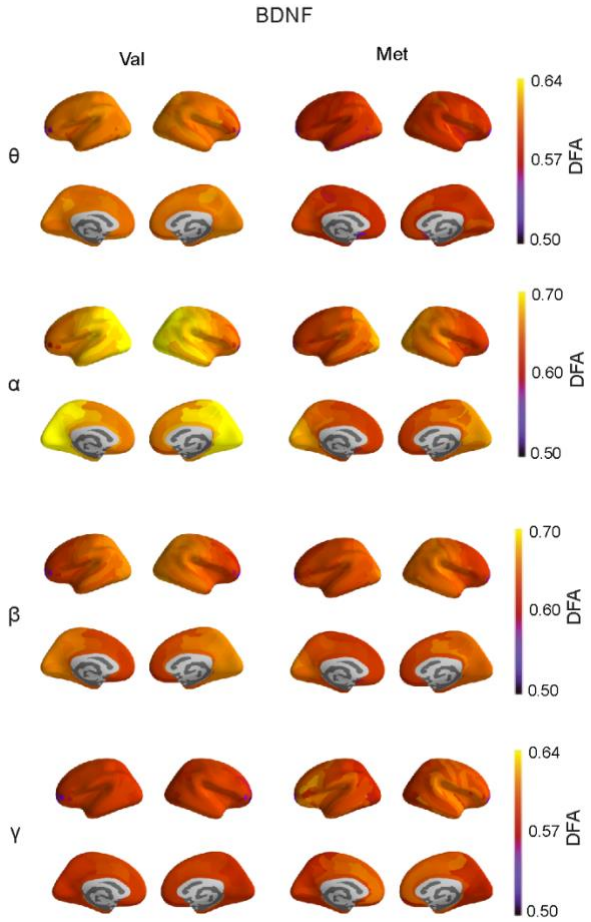

Fig S8. Mean LRTCs for *BDNF* polymorphisms. Mean DFA exponents are plotted separately for each *BDNF* polymorphism (Val/Val and Met-carriers) groups averaged over theta (θ, 3–7 Hz), alpha (α, 8–14 Hz), beta (β, 14–30 Hz), and gamma (γ, 30–60 Hz) frequency bands plotted on inflated cortical surface. The color indicates the strength of the DFA exponents. Note that the scales vary across frequency bands.

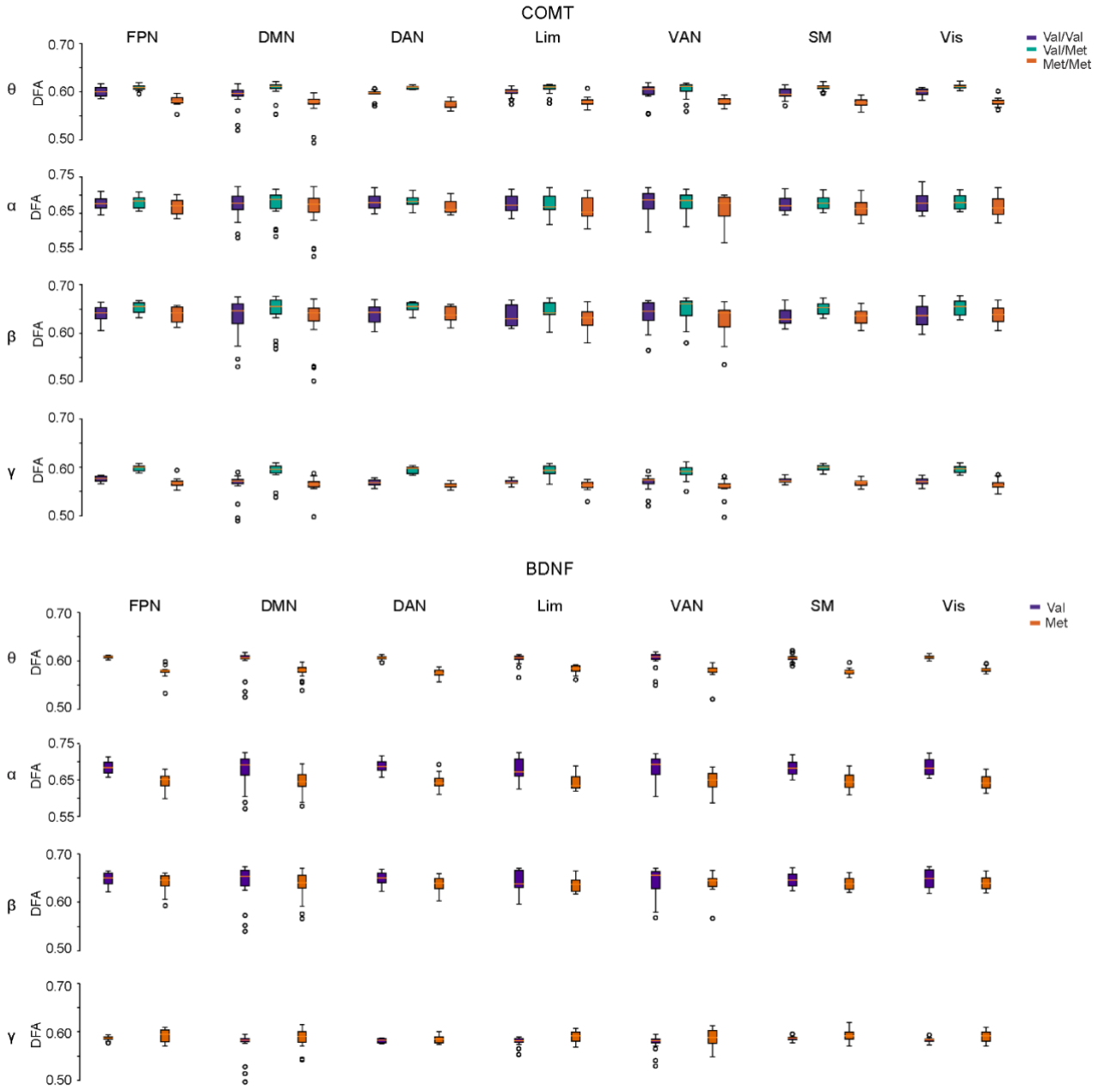

Fig S9. Mean DFA exponents across the functional subsystems. Box plots of DFA exponents averaged over the functional subsystems defined by fMRI functional connectivity across the frequency bands: theta (θ, 3–7 Hz), alpha (α, 8–14 Hz), beta (β, 14–30 Hz), and gamma (γ, 30–60 Hz) and separately for each *COMT* (Val/Val, Val/Met, and Met/Met, upper panels) and each *BDNF* (Val/Val and Met-carriers, lower panels) polymorphism groups. Abbreviations of the functional subsystems as in S5 Fig and box plot details as in S2 Fig.

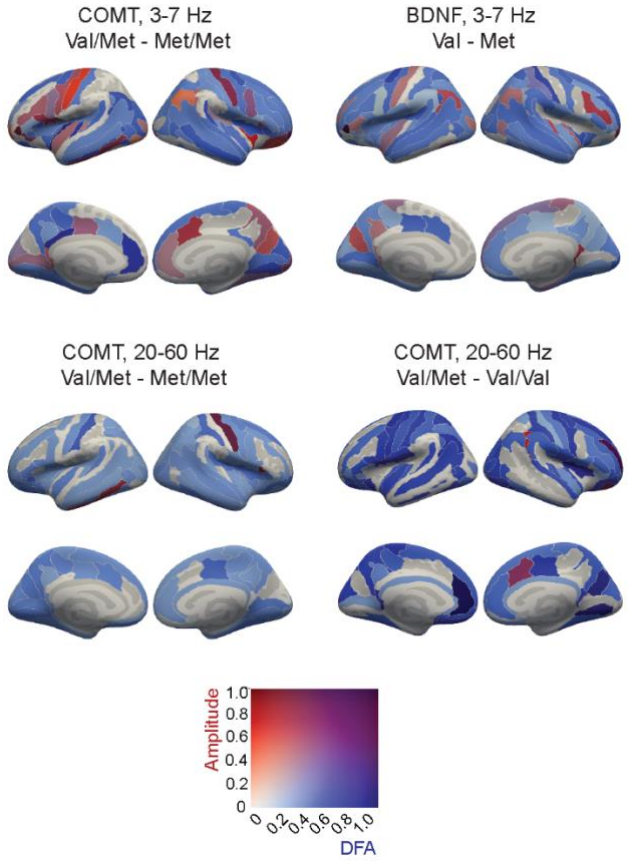

Fig S10. Co-localization of oscillation amplitudes and LRTCs. Cortical parcels in which amplitudes and DFA exponents were significantly larger for *COMT* Val/Met than Met/Met polymorphism groups in θ (3–7 Hz, upper left panel) and in β-γ (20–60 Hz, lower left panel) band, and for *BDNF* Val homozygotes than Met-carriers in θ (upper right panel), as well as for *COMT* Val/Met than Val/Val polymorphism groups in β-γ (lower right panel). The color indicates the difference in oscillation amplitudes (red) and DFA exponents (blue), as well as their joint effects (purple).

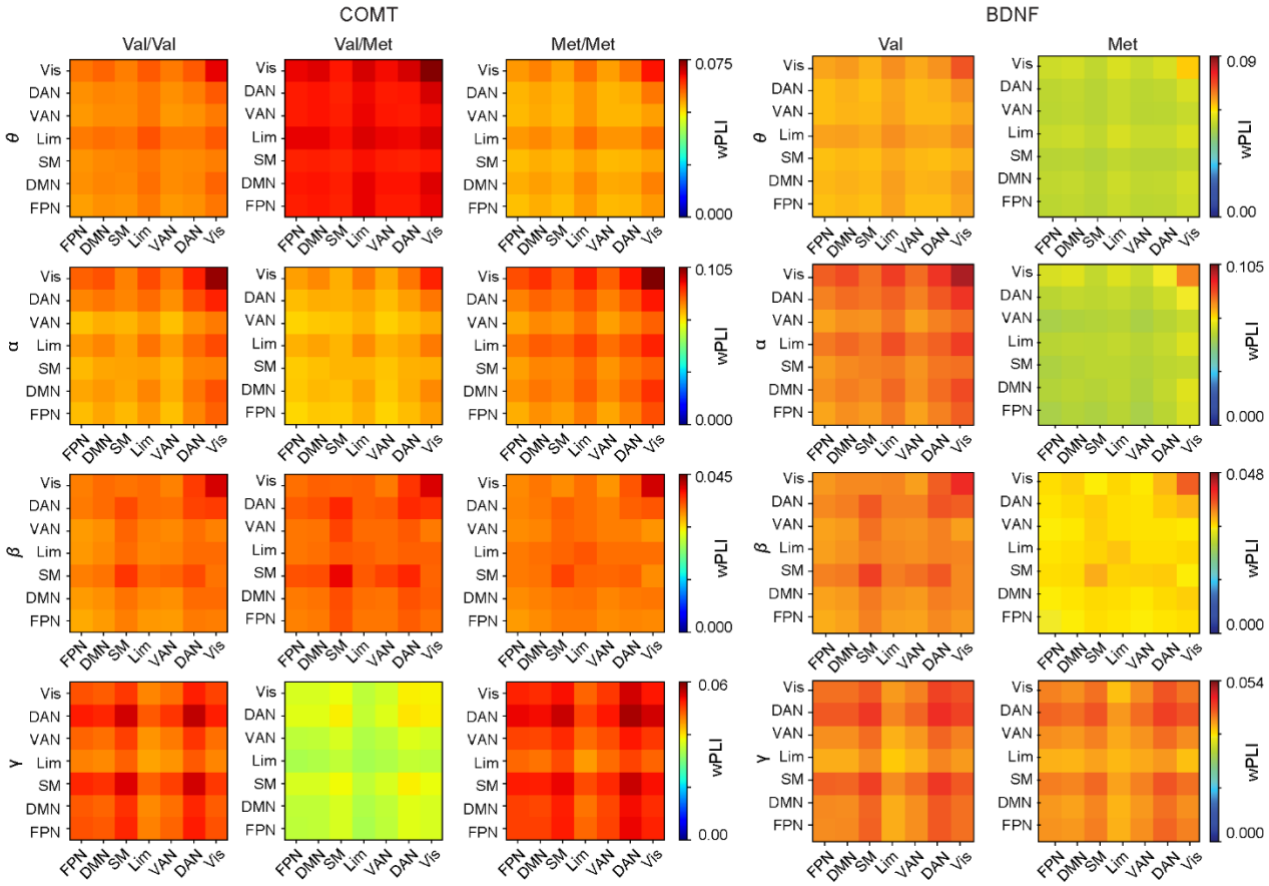

Fig S11. Phase synchronization associated with *COMT* and *BDNF* polymorphisms. The mean phase-synchronization within and among functional Yeo subsystems across the whole brain in the canonical frequency bands for the *COMT* Val/Val, Val/Met and Met/Met polymorphism groups and the *BDNF* Val/Val alleles and Met carriers. Inter-areal phase phase-synchrony was estimated between and within functional subsystems using the weighted phase-lag index (wPLI), of which the strength is indicated by the color scales. No differences in inter-areal phase coupling were found between *COMT* polymorphisms. *BDNF* Val/Val alleles showed stronger synchronization than Met carriers particularly in the α, β and γ bands, these differences are shown in Fig 4C. Note that the scales vary across the frequency bands. Abbreviations of the functional subsystems as in S5 Fig.

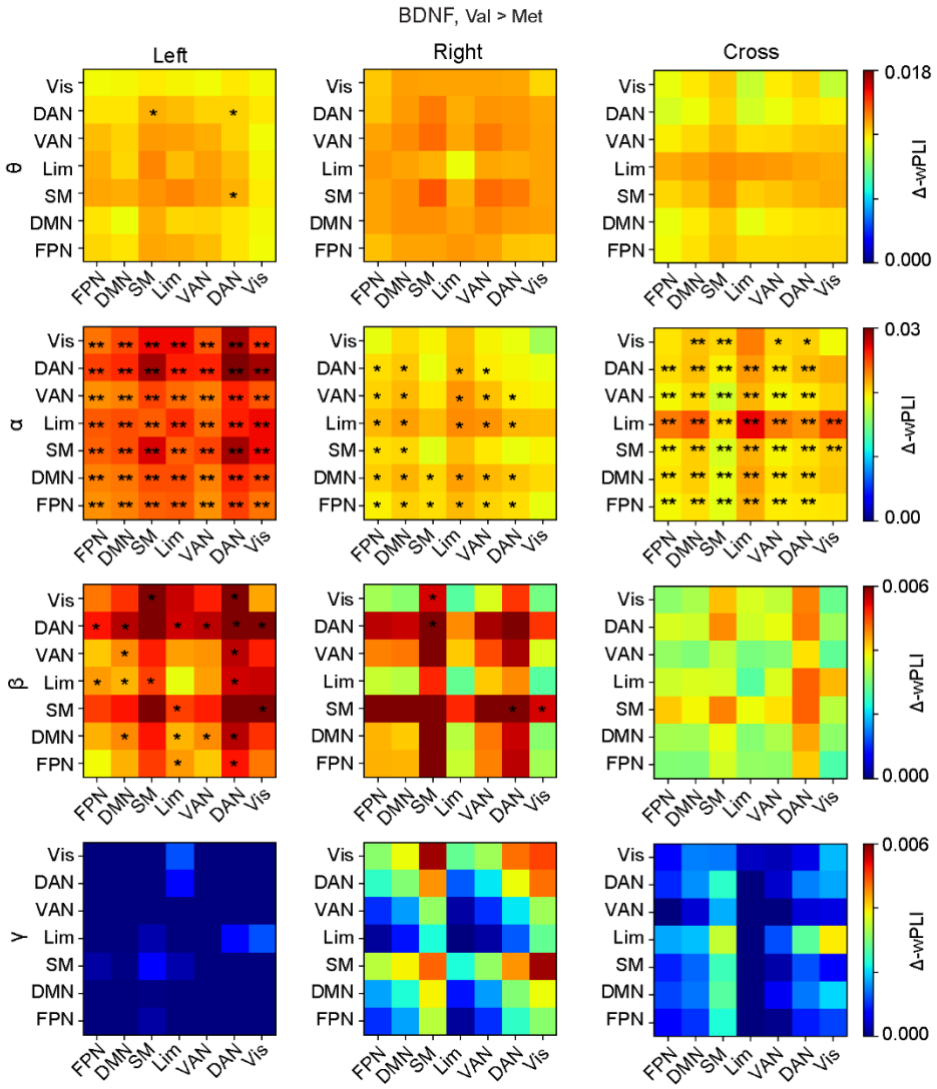

Fig S12. Hemispheric phase synchronization for the *BDNF* polymorphism groups. The differences in the mean phase synchronization, as estimated with wPLI, within and between functional subsystems separately for left-, right- and cross-hemispheric connections. *BDNF* Val/Val homozygotes had stronger phase synchronization compared to Met-carriers averaged over frequency bands. Color indicates the Val > Met difference in mean phase-synchronization. Stars denote network pairs where the group difference was significant (Kruskal-Wallis, *: $p < 0.05$**,** uncorrected, **: $p < 0.01$, corrected with Benjamini-Hochberg). Abbreviations of the functional subsystems as in S5 Fig.

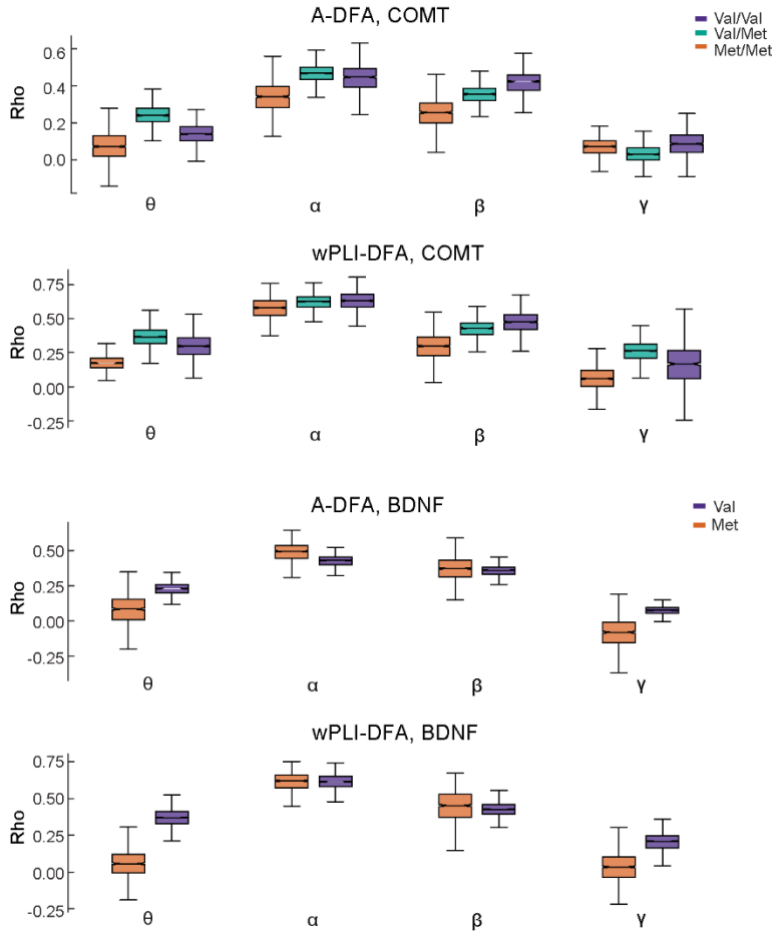

Fig S13. Correlations of local and global synchronization with LRTCs. Box plots of correlations of between A and wPLI with DFA exponents averaged over theta (θ, 3–7 Hz), alpha (α, 8–14 Hz), beta (β, 14–30 Hz), and gamma (γ, 30–60 Hz) frequency bands. Correlations are shown separately for each *COMT* (Val/Val, Val/Met, and Met/Met, upper panels) and each *BDNF* (Val/Val and Met-carriers, lower panels) polymorphism group. Box plot details as in S2 Fig.

Table S1. Mean sample characteristics (SD in parentheses) by the *COMT* polymorphisms.

	Val/Val	Val/Met	Met/Met
N	18	48	16
Age mean, years [1]	30.65 (9.90)	28.53 (8.91)	29.87 (10.69)
Age range	22–55	19–50	18–53
Handedness (right/left) [2]	18/0	41/5[1]	15/1
Gender (Female/Male) [3]	11/7	27/21	6/10
Rs mean, minutes [4]	7.86 (2.20)	7.97 (3.28)	7.49 (2.69)
Rs range	5–10	5–24	5–12

[1] Age information missing from three participants. The polymorphism groups did not differ in terms of age as confirmed by a one-way ANOVA.
[2] Handedness information missing from two participants.
[3] The percentages of female and male participants did not differ within the *COMT* polymorphism groups as indicated by the Chi-squared test.
[4] Rs = resting state. The duration of the resting state recording did not differ between polymorphism groups as confirmed by a one-way ANOVA.

Table S2. Mean sample characteristics (SD in parenthesis) by the *BDNF* polymorphisms.

	Val/Val	Val/Met + Met/Met
N	66	16
Age mean, years [1]	29.95 (9.26)	26.44 (9.69)
Age range	18–55	20–52
Handedness (right/left) [2]	59/6[2]	15/0[2]
Gender (Female/Male) [3]	35/31	9/7
Rs mean, minutes [4]	7.92 (3.07)	7.58 (2.47)
Rs range	3–24	5–10

[1] Age information missing from three participants. The polymorphism groups did not differ in terms of age as confirmed by an independent samples *t*-test (2-tailed).
[2] Handedness information missing from two participants.
[3] The percentages of female and male participants did not differ within the *BDNF* polymorphism groups as indicated by the Chi-squared test.
[4] Rs = resting state. The duration of the resting state recording did not differ between polymorphism groups as confirmed by an independent samples *t*-test (2-tailed).